2

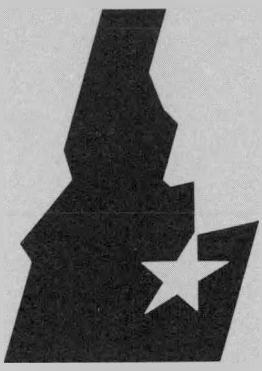

Idaho
National
Engineering
Laboratory

Managed
by the U.S.
Department
of Energy

EGG-BNCT-8319
May 1989

INFORMAL REPORT

NON-REACTOR NEUTRON SOURCES FOR BNCT

T. J. Dolan
E. H. Ottewitte
E. E. Wills
W. A. Neuman
D. M. Woodall

EG&G Idaho

Work performed under
DOE Contract
No. DE-AC07-76ID01570

NON-REACTOR NEUTRON SOURCES FOR BNCT
EGG-BNCT-8319

EGG-BNCT--8319

DE89 016211

T.J.Dolan, E.H.Ottewitte, E.E.Wills, W.A.Neuman, D.M.Woodall

ABSTRACT

The focus of this study is the identification of key feasibility issues for the use of non-reactor neutron sources for Boron Neutron Capture Therapy (BNCT). Of the non-reactor neutron sources surveyed, the $^{7}Li(p,n)$ reaction appears to be the most favorable for producing epithermal neutrons for BNCT, and RFQ accelerators are best for producing the desired proton beam. At a proton energy of 2.5 MeV, the total neutron yield is 1.49×10^{-4} neutrons/proton, with a forward energy spectrum extending up to 780 keV and peaked at 500-600 keV. At I = 20 mA (the maximum cw current attained in RFQ accelerators so far), the total neutron yield would be about 1.86×10^{13} neutrons/s. Using a 20 cm BeO filter, the resultant neutron flux exiting the filter would be about 2×10^{9} neutrons/cm^2s. In comparison with a medical therapy fission reactor, the 20 mA accelerator system has

* a flux intensity at least 5 times lower, requiring an irradiation time at least 5 times longer,
* a much higher gamma intensity, which would probably require additional shielding, further reducing the neutron intensity,
* 30 % of the neutrons above 15 keV (vs. <10 % for the reactor), resulting in a higher fast neutron dose to healthy tissue,
* poorer spatial uniformity of the neutron beam, and
* greater angular divergence of the neutron beam (poorer collimation), resulting in a rapid decrease of flux with distance from the filter.

The possibility of overcoming these limitations by using more shielding and a higher beam current needs further study. RFQ accelerator technology is being developed to provide the desired proton beam parameters (~ 100 mA at 2.5 MeV). The effects of neutron beam energy spectra, beam contaminants, angular divergence, spatial variation, and beam rotation around the tumor need to be studied in detail, in order to evaluate the feasibility of accelerator-produced neutrons for BNCT.

Contents

Abstract.....1

Contents.....2

1.0 Introduction.....4
Background
Focus of this Study

2.0 Criteria
2.1 Neutron Beam Quality.....7
Optimum neutron energies for $^{10}B(n,\alpha)$ interactions
Optimum energies to avoid damage to healthy tissue
Penetration depth considerations
Comparison of neutron energy criteria
A definitive study of neutron beam quality
Considerations on gamma contamination in the beam
2.2 Criteria on Charged Particle Reactions.....15
Projectiles
Target criteria
Reaction Q-values

3.0 Non-Reactor Neutron Sources
3.1 Radioisotope Neutron Sources.....17
3.2 Physics of Neutron Production by Ions.....17
Neutron energy-angle correlation
Monoenergetic neutrons
3.3 Neutron-Producing Reactions.....19
Energetics
Cross sections
3.4 Spallation Neutrons.....25
3.5 Accelerators.....26
Medium energy accelerators
Low energy accelerators

4.0 A Proton-Lithium Neutron Source for BNCT
4.1 Source Calculations.....33
Neutron scattering in the target layer
Continuous slowing down approximation
Neutron energy
Thick target neutron yield
Method of integration
Range-energy relationship
Discussion
4.2 Target Issues.....47
4.3 Gamma Ray Production.....51
Gamma flux
$^{7}Li(p,p'\gamma)$ reactions
(p,γ) reactions
Decay gammas from ^{7}Be
Summary
4.4 Neutron and Gamma Flux at the Patient with a BeO Filter....56

5.0 Summary and Conclusions.....62

6.0 References.....64

1.0 INTRODUCTION

1.1 Background

Each year in the USA almost 80,000 people die of tumors which might be treated with Boron Neutron Capture Therapy (BNCT). This procedure involves doping the tumor with a boron compound and then irradiating it with neutrons. On the average, it takes about one $^{10}B(n,\alpha)$ reaction in the nucleus or 2.5 reactions at the cell surface to destroy a cell. This method was first suggested in the 1930's, but adequate neutron sources, boron delivery compounds and monitoring were not available.

The glioblastoma multiforme type of brain tumor is a good candidate for early trials on humans. It is always fatal, with a life expectancy of less than a year using current treatment modalities. It cannot be treated successfully by other therapies, because many small tendrils extend into surrounding healthy tissue. These tendrils are very difficult to locate and to remove surgically without excessive damage to healthy brain tissue, and conventional radiation therapy is not feasible.

BNCT has been tried on humans with varying success. Early experiments using only thermal neutron beams produced high surface doses relative to the tumor dose. The boron compounds, which did not selectively dope the tumor, produced a high boron concentration in healthy tissue. There was no means of measuring the boron content in the patient. Fluid pressure induced by the therapy was not diagnosed and treated. As a result of these deficiencies, the early treatments at MIT were unsuccessful. Dr. H. Hatanaka has treated approximately 100 patients in Japan over the past 16 years, with varying success.[1]

Recently the situation has improved: diagnostics can now monitor boron content and fluid pressure; the compound sodium borocaptate ($Na_2B_{12}H_{11}SH$) concentrates preferentially in tumors; and epithermal neutron sources are available for irradiation.

For maximum effectiveness, BNCT requires incident neutrons with energies above 1 eV. Lower energy neutrons give a high surface dose without penetrating well into the tumor. Neutron energies above 10 keV are undesirable, because they produce considerable fast-neutron dose to healthy tissue. (For deep-seated tumors, multi-MeV neutrons have been used, with healthy tissue damage minimized by rotating the beam about the patient's tumor. The combination of such fast-neutron therapy with BNCT has not yet been attempted.)

A short irradiation time is best, because the boron in the tumor gradually depletes; some patients need constant attention, which cannot be given during irradiation; and the patient case load is expected to be high. A collimated flux at the patient of about 10^{14} neutrons/m^2-s is desirable to keep the required irradiation time down to about 10 minutes. The Power Burst Facility (PBF) can provide this flux, with little fast or thermal neutron contamination.[2] An advanced Medical Therapy Reactor has also been designed.[3] An accelerator source of neutrons for BNCT has been studied by the Ohio State University.[4] Figure 1 describes other potential sources of epithermal neutrons.

1.2 Focus of this Study

The goal of the present work is to determine whether non-reactor neutron sources could also satisfy the BNCT requirements and be more amenable to a hospital setting. We do not consider fusion reactors, because that technology is not yet developed.

Section 2 develops a set of criteria for a basis of comparison and selection. Section 3 examines various potential neutron sources. Section 4 examines epithermal neutron production with an RFQ accelerator and the ^{7}Li(p,n) reaction. The neutron and gamma fluxes to the patient are calculated for the case of a thin BeO neutron filter, and compared with the results of other groups.

Fig. 1 Neutron Sources

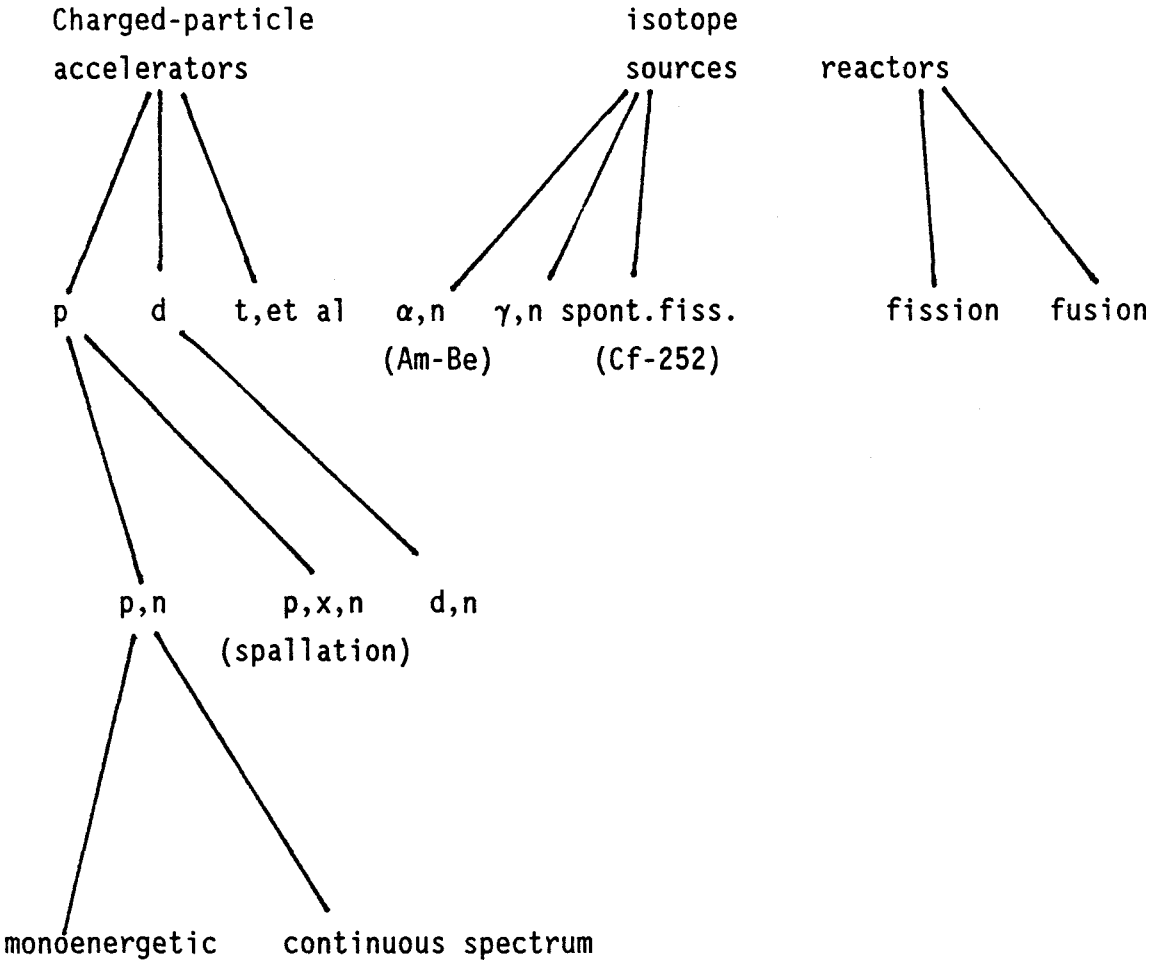

2.0 CRITERIA

2.1 Neutron Beam Quality

Optimum Neutron Energies for $^{10}B(n,\alpha)$ Interactions

For BNCT, the cross section for $^{10}B(n,\alpha)$ should be high enough to absorb most of the neutrons in the boron loading, without self-shielding the innermost portions of the tumor. To achieve a mean free path of 1 cm with a 25 ppm ^{10}B loading, a $^{10}B(n,\alpha)$ cross section of $7x10^5$ barns would be needed, which would occur only at neutron energies below 10^{-5} eV, as can be seen in Figure 2. Thus, most of the neutrons will pass through the boron-loaded tumor without interaction. We therefore prefer neutron energies <u>at the tumor site</u> as low as possible, for maximum interaction with ^{10}B.

Optimum Energies to Avoid Damage to Healthy Tissue

The rate of damage to tissue by neutrons is

$$D = K * QF$$

where

K = the KERMA rate (kinetic energy release in materials)

QF = neutron quality factor

Figure 3 shows the KERMA and product damage rate D as functions of neutron energy. Their minima occur at about 20 eV.

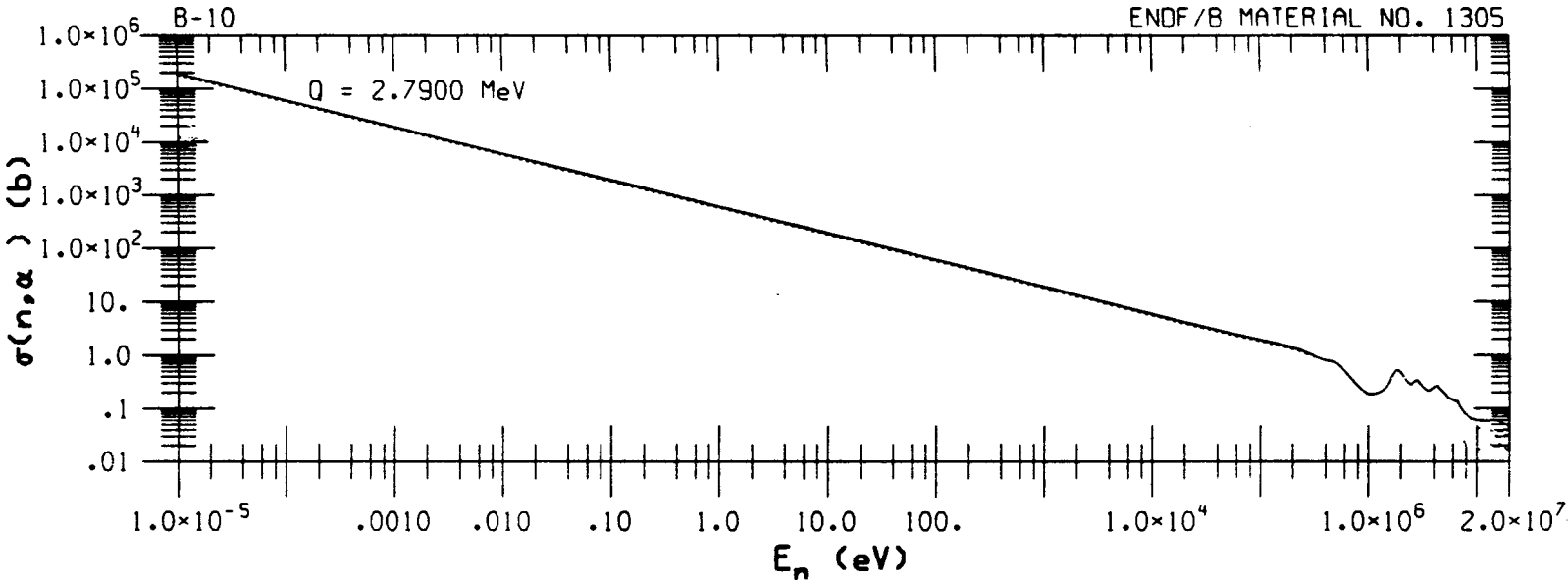

Fig. 2. Variation of the $^{10}B(n,\alpha)$ cross section with neutron energy.

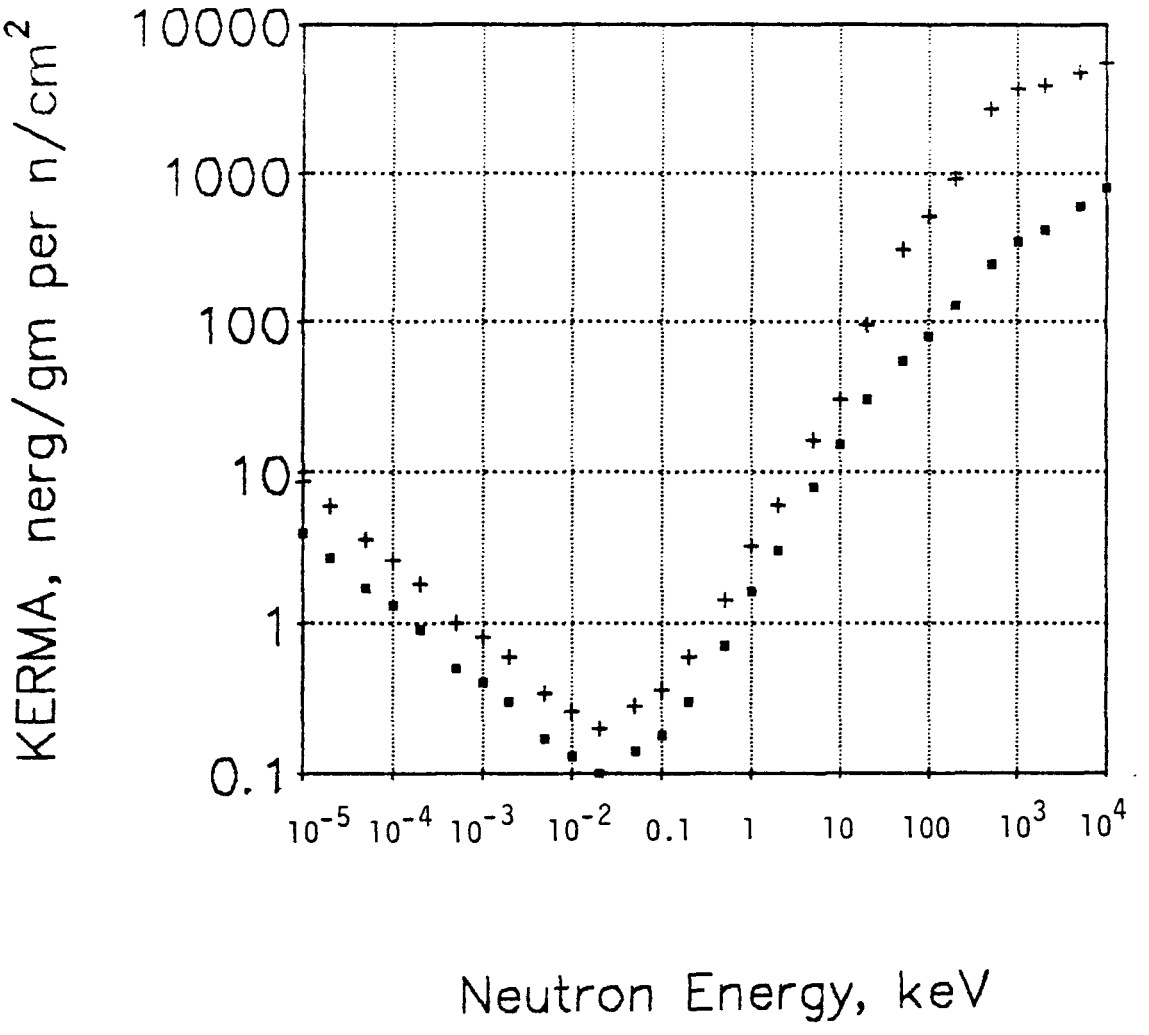

Fig. 3. Variation of KERMA (bottom curve) and tissue damage rate (top curve) with neutron energy.

Penetration Depth Considerations

The mean free path for thermal neutrons in H_2O is 0.37 cm, mostly due to the hydrogen scattering cross section σ_H, which is shown in Figure 4. From 0.1 to 10^4 eV the cross section remains constant at about 20 b. A consequence of this large scattering cross section is that many neutrons reflect back out of the head and many diffuse sideways. Few penetrate forwards. Above 100 keV, penetration increases, but so does healthy tissue damage.

Figure 5 shows how the thermal flux spatial distribution $\phi_{th}(r)$, depends on incident neutron energy. The thermal neutron flux from incident 1.4 eV neutrons peaks at about 1.9 cm; from 29 keV neutrons, at 3.4 cm; and from 1/E neutrons, at an intermediate depth. Apparently E_n >29 keV would be needed to make the thermal flux peak depth > 4 cm. Similar results are found in a study by Fairchild.[6]

Oka et al reported a BNCT study of dose-depth distributions.[7] They concluded

1) 10 eV < En < 500 eV are suitable energies for BNCT
2) Maximum Usable Depth for epithermal neutrons = 7 cm
   for thermal neutrons = 5 cm.

For deep tumors, one could irradiate patients with a narrow energy band of fast neutrons whose energy produces a thermal neutron peak at the tumor depth. (If slower neutrons were incident, some of them would be absorbed at shallower depths, causing damage to healthy tissue without reaching the tumor.) Morstin et al found the neutron beam energy maximizing the dose to a 1 cm diameter boron-loaded tumor at the center of a 30 cm diameter spherical tissue phantom to be 500 keV.[8] At that energy hydrogen absorption and proton recoil are both reduced. However, damage to healthy tissue may be excessive. It would be desirable to rotate either the patient or the neutron source around the tumor, in order to spread out the non-tumor dose, as is done with gamma therapy. Neutron diffusion would still spread out the dose over a large volume, as needed to kill tumors with long tendrils. This procedure might combine the advantages of fast neutron therapy and BNCT.

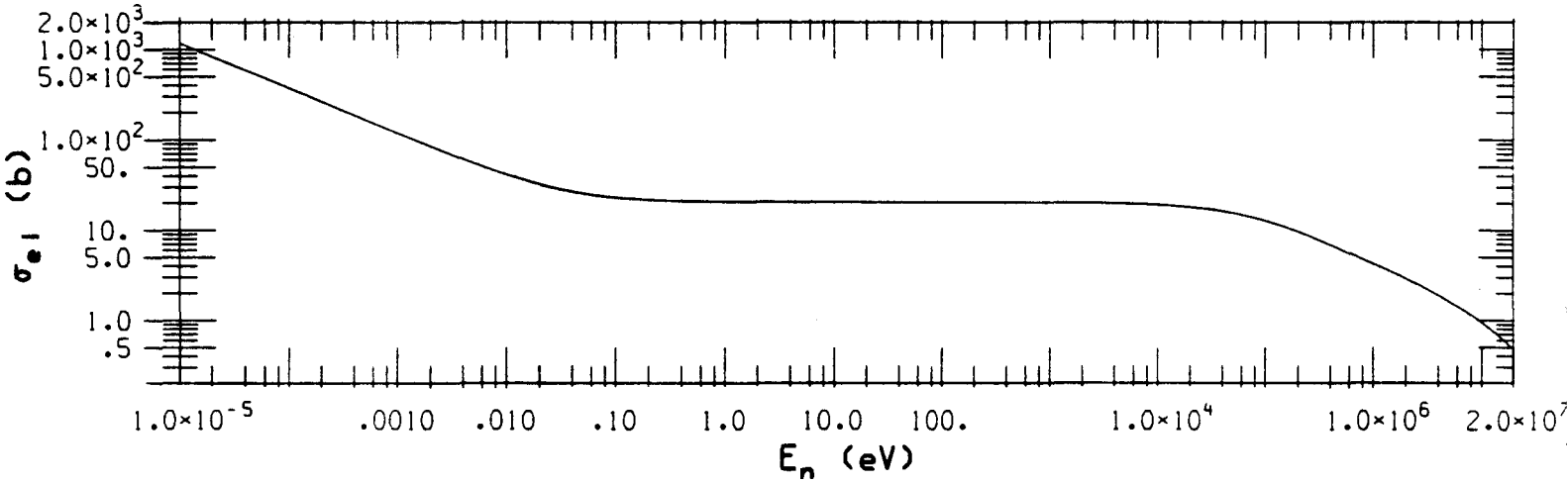

Fig. 4. Variation of hydrogen scattering cross section with neutron energy.

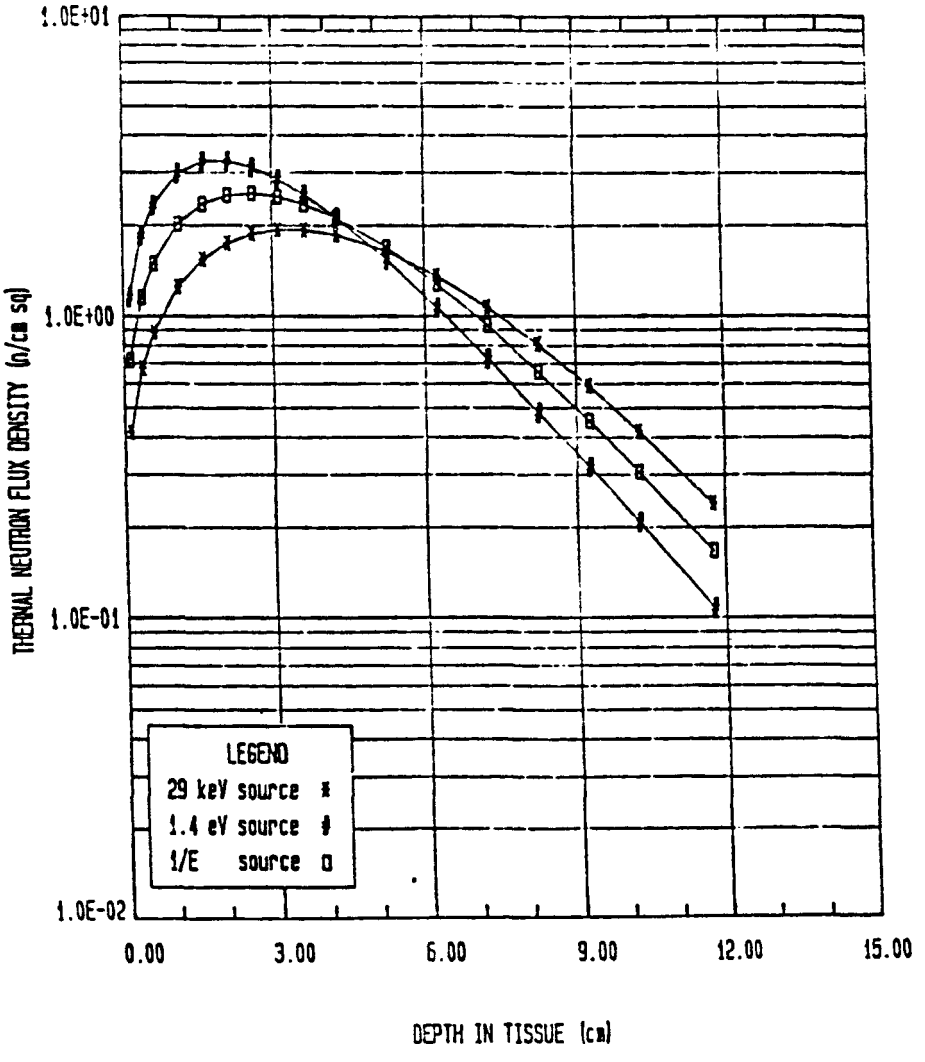

Fig. 5. Thermal flux with depth in phantom 16.6 cm diameter beam, tissue equivalent. [5]

Comparison of Neutron Energy Criteria

The optimum neutron energy ranges suggested by various groups are summarized below:

Oka [7]	0.01 - 0.5 keV
OSU Group [9]	0.001 - 1 keV
PBF Group [2]	0.001 - 10 keV
Uppsala/SIN Group [10]	1 - 10 keV
Morstin [8]	500 keV for deep-seated tumors

It appears that 10 keV is a practical upper limit for most BNCT. However, deep-seated tumors may need higher energy neutrons. A study of neutron interactions with tissue phantoms is beyond the scope of the present work.

A Definitive Study of Neutron Beam Quality.

A systematic study of the efficacy of various neutron energies, using several figures-of-merit, is desirable. This study would examine the effects of monoenergetic neutrons on both healthy tissue and tumors at various tumor depths. In this way the optimum neutron energy spectra could be determined as a function of tumor depth. An alternative procedure is to use a backwards (adjoint) transport theory calculation from the tumor back to the neutron source. This would reveal information on which neutron energies and pathways were most effective in destroying the tumor.

Gamma Contamination of the Beam

The process of producing a neutron beam from accelerated ions can also produce gamma photons. These may arise in various ways with neutron production reaction X(i,n)Y by

1)	X (i,nγ)Y	excitation of Y with prompt γ emission
2)	X(i,n)Y* -- β, γ, Z	excitation of Y with delayed γ emission
3)	X(i,γ)Z	(prompt)capture
4)	X(i,iγ)X	inelastic scatter, prompt emission
5)	X(i,i)X* -- β, γ, W	inelastic scatter, delayed emission

These reactions are also possible with other isotopes present in the target, so pure isotopic targets would be preferable. To avoid gammas from higher excited states of the product nucleus, ion energies should be kept below the thresholds for exciting those states. However, direct gammas from the accelerator target may be overshadowed by neutron activation gammas in the filter, shield, and patient.

2.2 Criteria on Charged Particle Reactions

Projectiles

The simplest projectiles are protons, deuterons, tritons and alpha particles. High energy electron beams can generate intense beams of gamma photons and photoneutrons; but some of the neutrons have high energies, and the photons would be difficult to shield for BNCT applications, so they are not considered further here. Heavy ions have intrinsic complexity of their reaction products, often leading to undesirable radioactivity.

Target Criteria

Target materials of high natural abundance would have low cost and minimal fast neutron and photon contamination from sister isotopes. The targets should be in a chemically-stable form (not prone to oxidize). Gases would have too low a density for effective interaction with the projectile beam, except at very high pressures. High pressures would require thick windows between the target and the accelerator vacuum, and the windows would attenuate the accelerator beam excessively, in addition to overheating. Issues of target heating, lifetime and vapor pressure will be discussed in Section 4.2.

Reaction Q-Values

The Coulomb Barrier to nuclear reactions is given approximately by

$$V = 0.5\ z\ A^{2/3}\ \text{MeV}$$

where z is the charge number of the projectile and A is the atomic number of the target nucleus. For example, for a proton (z = 1) incident on lithium (A = 7), the barrier is roughly 1.8 MeV. To penetrate this barrier and achieve appreciable nuclear interactions, the projectile needs an incident kinetic energy $E_0 > V$. The kinetic energy of the emerging neutron will be on the order of $(E_0 + Q)$, where Q is the nuclear energy released by the reaction.

Reactions with $Q > 0$ will produce neutrons with MeV energies, which would result in high tissue damage rates. To keep the neutron energies less than 1 MeV, it is desirable to have Q less than about - 0.5 MeV.

It is also desirable to keep the projectile beam energy low, in order to minimize accelerator size, power costs, and target heating. This precludes reactions with large negative Q values ($Q < -3$ MeV). Therefore, we will seek charged particle reactions having $-3 < Q < -0.5$ MeV.

3.0 Non-Reactor Neutron Sources

3.1 Radioisotope Sources

The ability to surgically insert or surface-attach a neutron source near a tumor (brachytherapy) might override other limitations in some cases. In general, (α,n) reactions produce MeV neutrons. One exception is with Li targets, because the small atomic mass of the product nucleus permits it to carry a larger share of the exit channel energy. This reaction has a maximum neutron energy on the order of 1 MeV and a most probable neutron energy of about 200 keV, so it deserves further consideration.

Neutrons from $Be(\gamma,n)$ sources also produce MeV neutrons, but gamma rays are undesirable. Energy spectra from $Li(\gamma,n)$ reactions have not yet been found.

Spontaneous fission sources produce MeV neutrons, with spectra harder than fission spectra. Although they produce MeV neutrons, they have been considered for BNCT.[11] The very low intensity of radioisotope sources makes them impractical for most BNCT applications.

3.2 Physics of Neutron Production by Ions

Neutron energy-angle correlation

Direct nuclear reactions include

a. elastic scatter, such as (p,p)
b. inelastic scatter, such as $(p,p'\gamma)$
c. stripping, such as (d,n)
d. (pionic) charge exchange, such as (p,n)
e pickup reactions, such as (p,d)
f. knockout reactions, such as (p,n), at high energies.

In direct reactions, a compound nucleus is not formed. In reactions (a) through (e), the same nucleon has actually gone right through (or by) the nucleus. Only in (f) was the incident projectile caught in the nucleus (via a single billiard ball collision if a direct reaction.)

When a compound nucleus is formed, the neutron emission is roughly isotropic in the center-of-mass (CM) coordinate system, which means forward-peaked in the laboratory system. Direct reactions retain the sense of direction: neutrons exit predominately forward in both the CM and laboratory systems. Direct reactions predominate in light nuclei where nuclear binding is not saturated.

Monoenergetic Neutrons

If the ideal neutron energy for BNCT were known for a given tumor depth, then it might be desirable to produce a beam of monoenergetic neutrons at that energy. The ideal energy might be close to the energy which produces a thermal neutron flux peak at the tumor depth (Figure 5).

Since the neutron intensity from charged particle reactions is usually strongly forward-peaked, it is most efficient to use those neutrons within a narrow cone in the forward direction. A narrow band of neutron energies could be obtained by using a thin target, but the neutron yield would be quite low.

It is also possible to achieve a narrow band of neutron energies by using incident charged particles with energies just above the reaction threshold. The neutron intensity is again low, because the charged particles traverse most of their slowing-down path with energies below the neutron production threshold.

The neutron energies will be spread out by any neutron energy filter or gamma shielding which is used, so it may not be fruitful to attempt to produce monoenergetic neutron beams. It is still desirable to avoid exceeding the energy for the first excited state of the product nucleus, in order to avoid high-energy gamma ray production.

3.3 Neutron-Producing Reactions

Energetics

Table 1 shows the Q values for most reactions of p,d,t, and alpha particles with light nuclei. For the case of deuteron projectiles, the C-12 and O-16 reactions look satisfactory. However, in these cases there would be some contamination with high energy neutrons produced in the isotopes C-13, O-17, and O-18, unless pure isotopes C-12 and O-16 were used.

For the case of triton projectiles, only the reaction with ordinary hydrogen looks favorable. There could be some production of high-energy neutrons from the 0.015 % of deuterium present in ordinary hydrogen, and this reaction is done more easily using tritium as the target and protons as projectiles.

For the case of alpha particle projectiles, the isotopes O-18 and F-19 look energetically feasible. However, the small abundance of O-18 means that the yield from naturally-occurring oxygen would be very small. Lithium-6 is marginal.

The case of proton projectiles looks most promising. Since the isotopes C-13, N-15, O-17, and O-18 all have very low abundances, they are less useful than the other reactions. Among the light elements, targets of tritium, Li-7, Be-9, B-11, and F-19 are most promising from the standpoint of Q values and abundances.

In addition, a few (p,n) reactions with heavier elements have been found useful for producing low-energy neutrons. Some of these are listed below, with their threshold proton energies (MeV):

Sc-45	2.908
V-51	1.566
Fe-57	1.648
Cu-63	4.214
Cu-65	2.14 .

Table 2-1. Q Values, MeV, for (x,n) nuclear reactions among light elements. [12-14]

		projectile			
target	% abundance	protons	deuterons	tritons	alphas
hydrogen	99.985		-2.225	-0.764	-23.489
deuterium	0.015	-2.225	3.269	17.590	-4.191
tritium	negligible	-0.764	17.590	10.439	-4.784
He-3	0.00014	....	-5.134	10.131	-9.091
He-4	99.99986	-23.489	-4.191	-4.784	-18.992
Li-6	7.5	-5.070	3.382	16.026	-3.975
Li-7	92.5	-1.644	15.032	10.439	6.632
Be-9	100.	-1.850	4.361	9.559	5.702
B-10	19.9	-4.434	6.466	18.931	1.059
B-11	80.1	-2.764	13.733	12.423	0.159
C-12	98.90	-18.121	-0.291	4.016	-8.502
C-13	1.10	-3.003	5.326	9.903	2.215
N-14	99.63	-5.927	5.073	14.479	-4.735
N-15	0.37	-3.536	9.903	7.790	-6.410
O-16	99.762	-16.211	-1.624	1.270	-12.135
O-17	0.038	-3.543	3.382	7.557	0.587
O-18	0.200	-2.439	5.769	6.113	-0.697
F-19	100.	-4.021	10.620	11.125	-1.951

The next step is to examine the cross sections of the energetically interesting reactions.

Cross Sections

The cross sections for various reactions are given in Table 2.

Table 2. Reaction cross sections.

target	E_{th} MeV	suitable E, MeV	typical σ, mb	
$^{3}H(p,n)$	1.0	2.0	300	[15]
$^{7}Li(p,n)$	1.88	2.5	500	[16]
$^{9}Be(p,n)$	2.1	2.7	120	[17]
$^{11}B(p,n)$	3.0	4.0	50	[17]
$^{12}C(d,n)$	0.3	1.5	(~ 10 mb/ster. at 0 degrees)	[19]
$^{19}F(p,n)$	2.9	3.8	50	[17]
^{45}Sc	2.9	3.0	(~ 2 mb/ster. at 0 degrees)	[18]
$^{63}Cu(p,n)$	4.2	4.3	(~ 2 mb/ster. at 0 degrees)	[18]

Since gas targets are undesirable, the lithium target appears to be the best choice among these elements. If high neutron energies were acceptable, then the $^{9}Be(d,n)$ reaction (not shown in Table 2) would provide a higher neutron yield.

Thick targets produce neutrons at energies corresponding to all projectile energies from incident energy to threshold. The thick-target yield from the $^{7}Li(p,n)$ reaction will be calculated in Section 4.

Considering only forwardly-directed neutrons, the differential cross section data of Table 3 are shown as a function of neutron energy in Figure 6. A significant upturn in the cross section begins at E_n = 350keV. This corresponds to the opening of the channel to the ^{7}Be $1/2^-$ level at 0.429 MeV (Figure 7), occurring at E_p = 1.644 + 0.429 = 2.07 MeV for the forward direction. The channel becomes fully open (at all angles) near the cross section peak at E_n = 570 keV (E_p = 2.3 MeV).

Table 3

$^{7}Li(p,n)$ Cross Section Data at Zero Degrees. [20]

E_p (MeV)	E_n (keV)	$d\sigma/d\omega$ at 0 degrees (mb/sr)
1.95	164	59
2.00	230	38
2.05	291	27
2.10	350	27
2.15	407	45
2.20	463	89
2.25	518	145
2.30	573	149
2.35	627	124
2.40	680	104
2.45	733	89
2.50	786	79
2.60	891	66

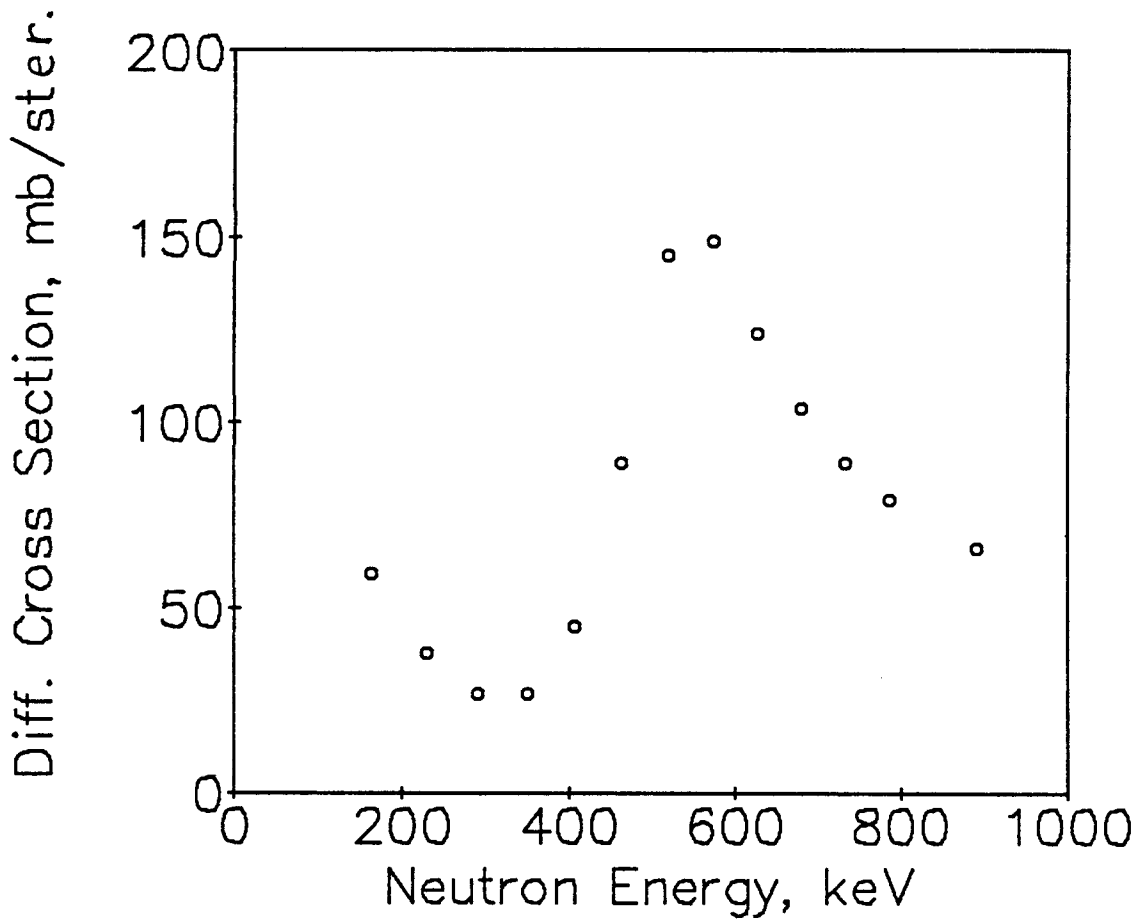

Fig. 6. Differential cross section of $^{7}Li(p,n)$ reaction at zero degrees as a function of resultant neutron energy.

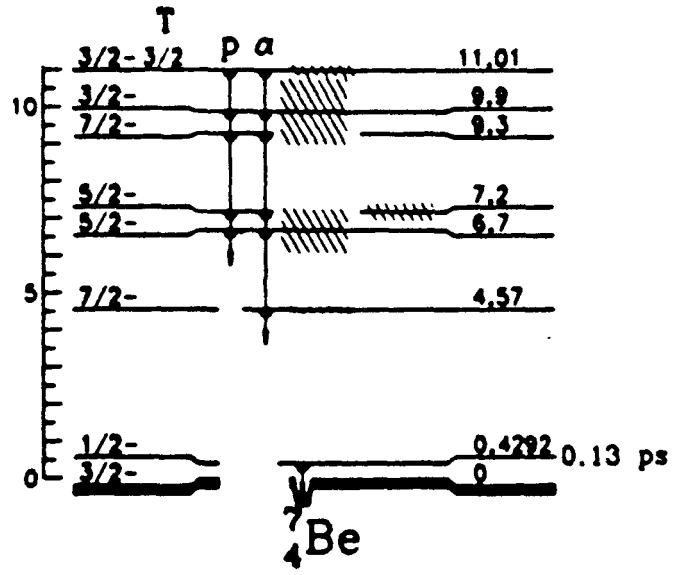

Fig. 7. Energy levels of ^{7}Be.

Thus, comparatively high neutron yields can be obtained by using incident proton energies above this peak.

3.4 Spallation Neutrons

An Uppsala/SIN collaboration has studied production of spallation neutrons using the 72 MeV proton beam of the SIN injector with a copper target.[10] Neutrons with a broad energy spectrum from low energy to almost the full energy of the protons are produced by spallation and direct reactions in copper. High energy neutrons produced in direct nuclear reactions are mainly emitted in the forward direction, while spallation neutrons with lower energies are emitted isotropically in the center-of-mass system. To reduce the fast neutron component several filter combinations were considered. A 75 cm radius iron sphere attenuated most of the neutrons above 1 MeV.[10]

Approximate neutron yields (neutrons per incident proton) for spallation targets at various proton energies are shown below:

	20 MeV	50 MeV	100 MeV	200 MeV	500 MeV
Be	0.02	0.08	0.23	0.4	1.4
Pb	< 0.01	0.06	0.35	1.5	7

Despite high proton energies, neutrons are mostly "boiled off". The proton energy goes mainly into neutron binding energy (releasing more neutrons), not into neutron kinetic energy. Since the yield increases rapidly with beam energy, high-energy beams produce less target heating per neutron emitted, but the high-energy accelerators are more cumbersome and expensive.

If spectra from spallation sources were acceptable, then a compact spallation source, such as the superconducting cyclotron for Detroit's Harper-Grace hospitals, could prove competitive; but spallation spectra generally have too many high energy neutrons.

3.5 Accelerators

Accelerators for medical therapy may be grouped into two general categories: low-energy accelerators (< 10 MeV) and medium-energy accelerators (> 10 MeV, for spallation sources). For production of a large-diameter BNCT neutron beam, the proton beam emittance requirements are considerably relaxed, compared with other accelerator applications. This might allow higher currents and lower costs in some accelerator concepts.

An accelerator for BNCT could be attractive if it had a compact size and a low cost. It could be more easily accomodated in urban hospitals than a larger, more expensive accelerator. Table 4 shows the state of accelerator technology for low and medium energies, pertinent to BNCT. Figure 8 shows these accelerators on a graph of beam voltage and current. Radiofrequency quadrupole (RFQ) accelerators can attain high currents with relatively compact sizes and low costs. Currents of 100 mA and higher are achievable, and 1000 mA are anticipated.[23]

Medium Energy Accelerators

For spallation neutron production, a superconducting cyclotron is attractive. The spallation neutrons are well suited to fast-neutron therapy, and they may be adaptable to BNCT, if the patient or beam is rotated.

Table 5 shows existing clinical fast neutron therapy facilities. The accelerator technology is available to use filtered spallation neutrons for BNCT in a hospital, if some high-energy neutrons could be tolerated. Advanced designs include

* a compact superconducting cyclotron for Detroit's Harper-Grace Hospitals. It will bombard Be with 10-20 μA of 50 MeV deuterons to produce neutrons with a maximum energy of 55 MeV and a peak at 25 MeV. Such a beam can deposit 50 Rad/min at 8 mm depth and 25 Rad/min at 14 mm. Its cost, if commercially marketed, will be about 3 M$.

Table 4. Accelerators pertinent to BNCT. [21]

Accelerator Class	Location	I, mA	V, MV	Size, remarks
Electrostatic Linacs				
Pressurized				
Van de Graaf	MIT	~1	8-9	10 m x 4m
Linac	HVEC	0.4	4	13 m x 7m 10^{12}n/s
	Columbia U.	0.1	4	
Tandem				
Van de Graaf	general	0.0005	12-30	2.4-91.5m
	MP, Yale	0.01	20	24.5 m
	NSF	0.6	30	
	Daresbury			
	Laddertron	0.5	30	~20m
Electrodynamic Linacs				
C-W Cascade		1-10	3-4	
Adv. C-W		< 1000	8-10	
Insulating Core				
Transformers (ICT)		25	1-3	
Dynamitrons		100	0.5	
Tandem Dynamitrons		100	4.5	
Cyclotrons				
Regular	Hospitals	0.1-0.2	8-66 p,d	
Superconducting	Detroit	0.02	50 d	3-4 M$
RFQ				
Present	LANL	10-20	2-2.5	1-2m
Developmental	Chalk River	100	2.5	
Future	ORNL	1000	2	5 m
Alvarez Linac		100	3.7	50m

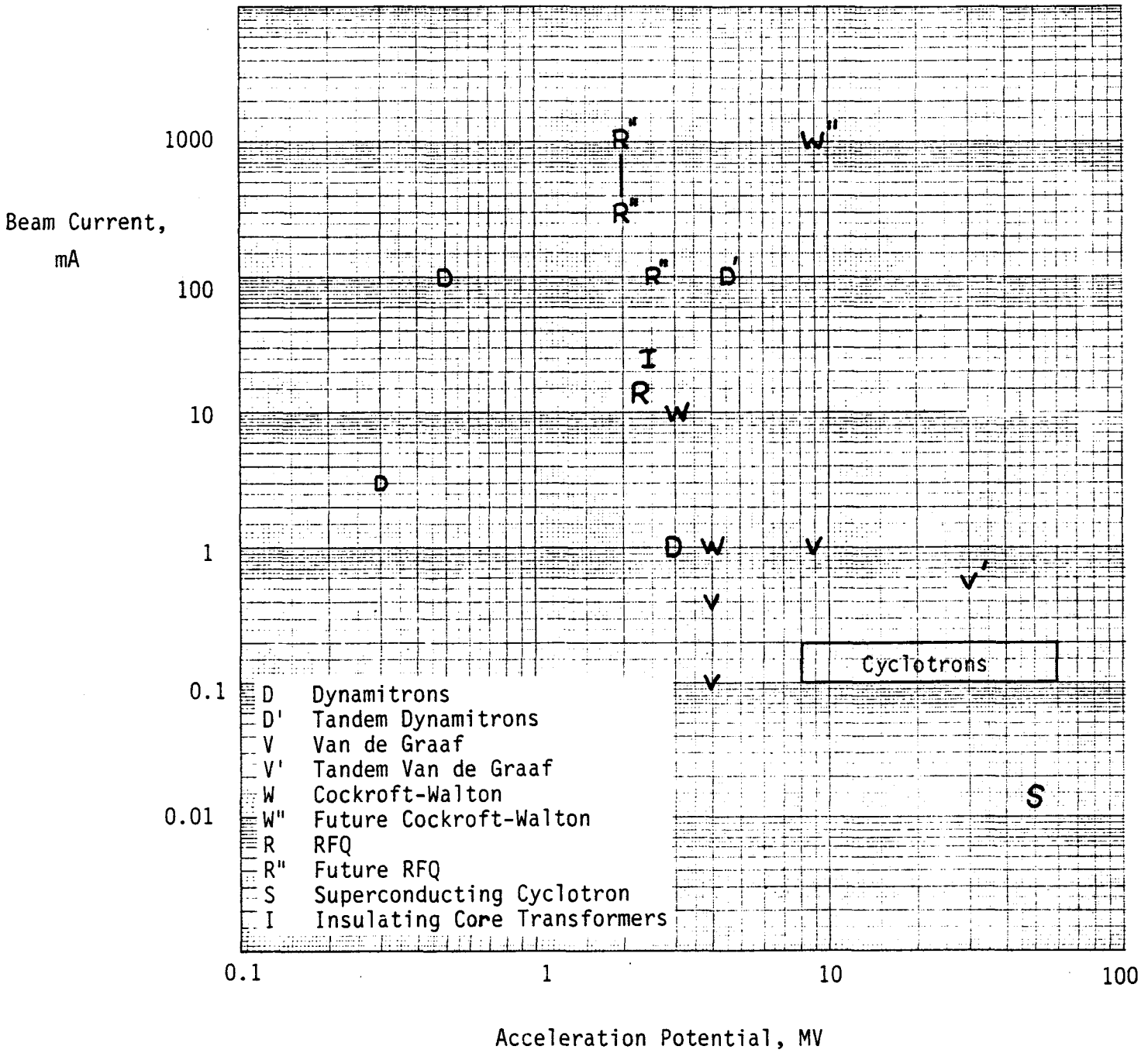

Fig. 8. Capabilities of present accelerator technology pertinent to BNCT.

Table 5. Clinical Spallation Neutron Facilities. [22]

Continent	Facility	Location	beam	Energy of Accelerated Particle (MeV)	Mean Neutron Energy (MeV)
USA	Fermilab*	Batavia Illinois	p + Be	66	25
	TAMVEC**	College Station, Texas	d + Be	50	19.3
	M.D.Anderson	Houston	p	42	
	NRL/MANTA* Geo.Wash.U.	Washington, D.C.	d + Be	35	14.3
	NASA/GLANTA	Cleveland, Ohio	d + Be(old) p (new)	25 42	10
	Univ. Wash.	Seattle, Wash.	d + Be(old) p (new)	22 50	8
	UCLA		p	46	
	Univ. of Chicago	Chicago, Ill.	d + d	8	6
U.K.	MRC, Hammersmith**	Liverpool London	p d + Be	60 16	7
	MRC, Edinburgh	Edinburgh	d + Be	15	6

Table 5, continued

	Facility	Location	Production Process	Energy of Accelerated Particle (MeV)	Mean Neutron Energy (MeV)
Europe	Antoni van Leuwenhoek Hospital***	Amsterdam	d + T	--	14
		Essen	d	14	
		Louvain	p	65	
		Dresden	d	13.5	
		Krakow	d	10.0	
		Orleans	p	34.0	
Japan		Sendai	p	50	
	NIRS+	Chiba	d + Be	30	12
	IMS++	Tokyo	d + Be	15	6
Middle East		Riyadh	p	26	

* proton linac 30 rad/min
** cyclotron
*** d-T generator and two small cyclotrons
\+ cyclotron 45 rad/min 70 MeV protons also accelerated
++ cyclotron 20 rad/min

* a Sandia design of a 200 mA, 0.2 MV d+ accelerator (tritium target) to produce 10^{13} n/s (14 MeV neutrons).

Low Energy Accelerators

Kapchinsky and Teplyakov (ITEP Moscow) proposed the radiofrequency quadrupole (RFQ) accelerator concept in 1970. It offered a new linear accelerator structure in which rf electric fields simultaneously focus, bunch, and accelerate an ion beam to 1-2 MeV/nucleon in a few meters distance. In the USA, LANL has extensively developed the concept for use as an injector to other accelerators, including a hospital-based pion source. Table 6 lists parameters of some recent designs. For acceleration to 2.5 MeV, currents of 10-20 mA cw and 100 mA pulsed have been achieved. AECL is presently attempting to achieve 100 mA CW.

Columbia University uses a 4 MV van de Graaf in their Radiological Research Accelerator Facility (RARAF) to accelerate 100 μA of protons.

Table 6. Recent RFQ projects

	E,MeV	beam	I, mA	Cost,M$	Remarks
Texas	2	p			
Kyoto U.	2	p			
Ohio State U.	2.5	p	10		
ACCSYS					Inj. to Loma Linda synchrotron
-PL-2	2	p	25	$1.5 M	Inj. to linac for PET isot. supply
-DL-1	0.9	d	5-15		FAA airport explosives detection
-	2.5	p	20		$>10^{12}$ n/s via Be(p,n) for Navy aircraft radiographical detection of structural fatigue and defects
-	2-2.5	p	0.4		for BNCT
-		p			Inj. to 4-5 MeV drift tube linac. Use with water-cooled Be to get $\phi_{th} = 10^{13}$ n/cm^{2}s for real time imaging of rocket motors
LANL					
-AT-2	2	p			Inj. to a 5 MeV drift tube linac
	2	d			FMIT design, 80 MHz, 100 mA max
-BEAR	1	H^-	0.5		Military space application interrogation, 20 mA peak
-GTA-1	2				
-Generic			10		State-of-the-art, 400 MHz,100 mA peak, 6-12% duty factor
-PIGMI	2.5	p	0.1		Inj., 28 mA peak current, 440 MHz
AECL	0.6	p	75		
-RFQ1	0.75	p	100		As of 10-4-88
-	2.5	p	10	$1 M	
-RFQA,RFQAT...	2.5	p	100		Advanced design,~3m long, 500-800 kW structure loss
SAIC-		d,He	0.1	<$1 M	RFQ+linac drift tube for PET isotope production, < 2 m
-	1	d			FAA bomb detection via neutron activation of N.
ORNL	2	p	1000		Goal for future tokamak plasma heating by neutral beam injection 5 m long [23]

4.0 A Proton-Lithium Neutron Source for BNCT

4.1 Source Calculations

Neutron Scattering in the Target Layer

On the average, a neutron would have to travel about half the thickness Δx of the source region to escape in the forward direction. The fractional neutron scattering and absorption in the thin target region where they are produced will be on the order of this distance divided by the neutron mean free path:

$$\text{scattering probability} \sim 0.5\Delta x/\lambda = 0.5 n_{Li} \sigma \Delta x$$

The total cross section σ of lithium for scattering and absorption of neutrons, shown in Figure 9, is about 1-2 barns, with a narrow peak ~ 12 barns at 0.27 MeV. Using a mean cross section ~ 3 barns and Δx ~ 90 μm, the scattering probability is estimated to be ~ 6×10^{-4}. Thus, the error caused by neglecting neutron scattering in the thin target region is negligible, and it is not necessary to calculate neutron transport through the source region of the target. We can treat the neutrons as if they all originated from the same source plane.

The Continuous Slowing-Down Approximation

The determination of the neutron source entails a solution of the Boltzmann transport equation, taking into account electronic effects, nuclear potentials, recoil energies, ionization, phonons, and so on. However, a simpler estimation can be made using the "continuous slowing down approximation", which is analogous to a fluid calculation (first moment of the Boltzmann equation). This calculation treats the protons as if they all decelerated at the same rate, with no deflections (no longitudinal straggling or lateral spread). The errors of this approximation are less than the uncertainty of the cross section data.

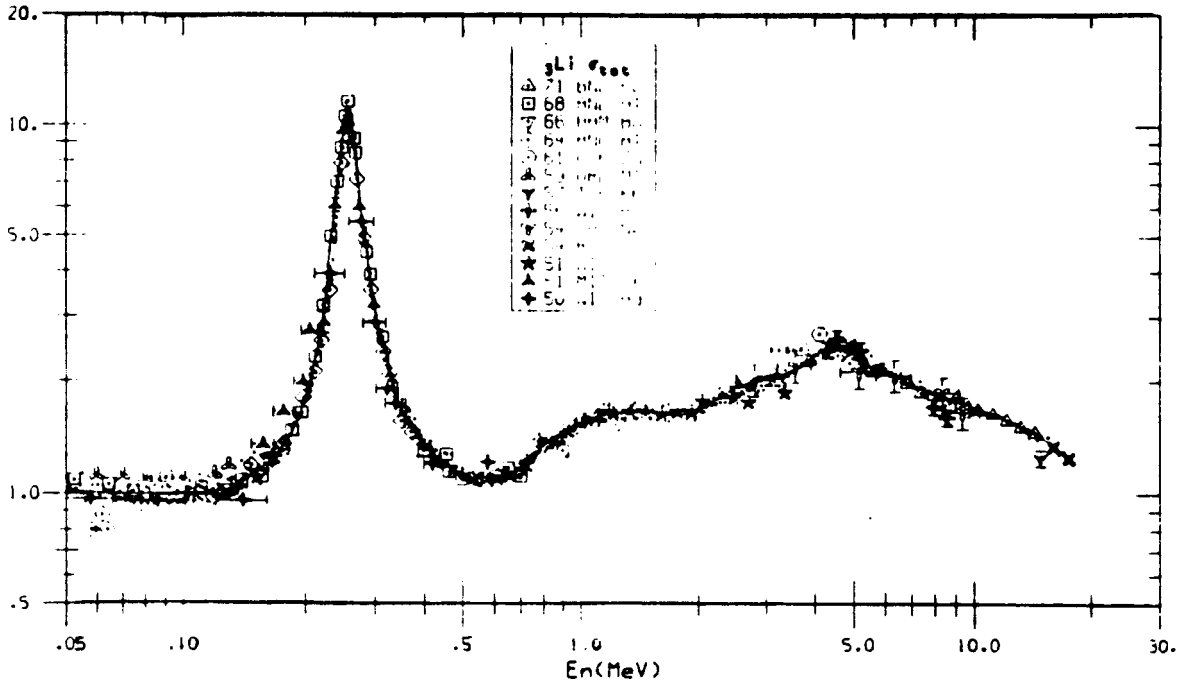

Fig. 9. Total cross section (barns) of natural lithium for neutrons vs. neutron energy.[24] The cross section for pure ^{7}Li is almost identical.

The stopping power of protons in solids is found from the algorithms of Andersen and Ziegler [25]:

$$(1/\rho)(dE_p/dx) = \begin{cases} 1.411\ E^{1/2} & \text{if } E < 10 \text{ keV/amu} \\ S_L S_H/(S_L + S_H) & \text{if } 10 < E < 1000 \\ (0.00153/\beta^2)[\ln(21470\beta^2/(1-\beta^2) - \beta^2 - SUM] & \text{if } E > 1000, \end{cases} \quad (1)$$

where

the units of $(1/\rho)(dE_p/dx)$ are 10^{-15}eV-cm^2/atom(Li)

$E = E_p(keV)/1.0073$ amu

$S_L = 1.60E^{0.45}$

$S_H = (725.6/E)\ln(1 + 3013/E + 0.04578E)$

$\beta^2 = v^2/c^2 = 1 - (E_p/935259.2 + 1)^{-2}$

$SUM = -0.5831 + 0.562\ln(E) -0.1182[\ln(E)]^2 + 0.009298[\ln(E)]^3 -0.0002498[\ln(E)]^4$

v = the proton velocity

c = the speed of light.

These equations can be integrated to find the relationship between proton energy and path length.

Neutron Energy

The following relativistic mass corrections are used [26]:

$$m_p = m_{po} + E_p/2c^2$$

$$m_n = m_{no} + E_n/2c^2$$

$$m_{Be} = m_{Beo} + E_{Be}/2c^2,$$

where subscripts o denote rest masses, and c is the speed of light.

For reasonable target temperatures, the lithium atoms may be assumed to be at rest. The neutron energy resulting from the (p,n) reaction is found from conservation of energy and momentum relations:

$$E_p + Q = E_n + E_{Be}$$

$$(2m_pE_p)^{1/2} = (2m_nE_n)^{1/2}\cos(\theta) + (2m_{Be}E_{Be})^{1/2}\cos(\phi)$$

$$0 = (2m_nE_n)^{1/2}\sin(\theta) + (2m_{Be}E_{Be})^{1/2}\sin(\phi)$$

where the lab angles of the neutron and recoil Be atom are denoted by θ and ϕ, respectively. If excited states of product nuclei are not produced, Q = -1644 keV. Eliminating E_{Be} and ϕ from these equations yields the "Q Equation"

$$Q = (1 + m_n/m_{Be})E_n - (1 - m_p/m_{Be})E_p - 2(m_pm_nE_pE_n)^{1/2}\cos\theta/m_{Be}. \qquad (2)$$

Given two of the parameters E_n, E_p and θ, the third can be found from this equation. For example, the solution for E_p may be written

$$E_p = [- x +(x^2 + y)^{1/2}]^2 \qquad (3)$$

where $x = (m_pm_nE_n)^{1/2}\cos\theta/(m_{Be} - m_p)$

$$y = [(m_{Be} + m_n)E_n - m_{Be}Q]/(m_{Be} - m_p).$$

The threshold proton energy is found by setting $E_n = 0$ in this equation, with the result

$$E_{th} = - m_{Be}Q/(m_{Be} - m_p) \sim 1881 \text{ keV}.$$

Near threshold, the relation of E_n to E_p bifurcates in the forward direction. The physical reason for this is illustrated in Figure 10.

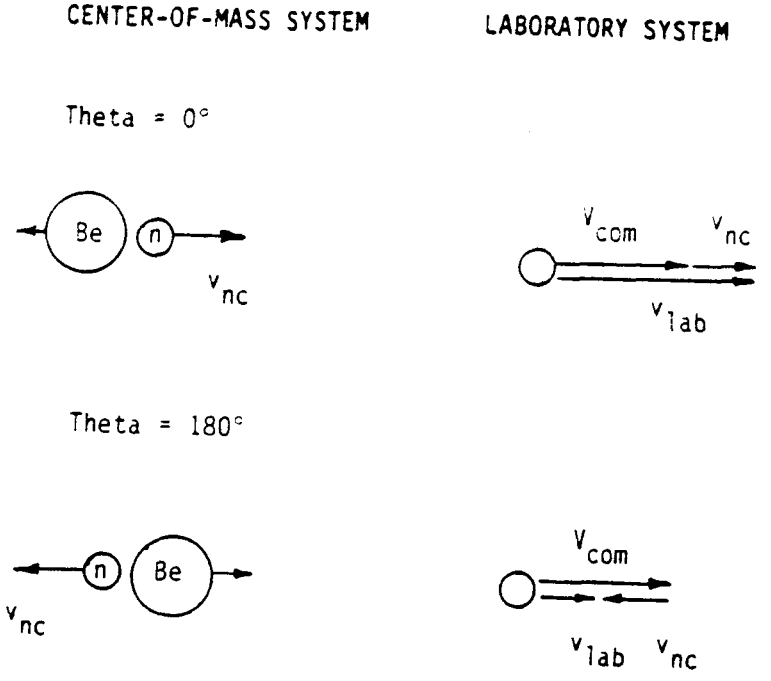

Fig. 10. The occurence of two neutron energy groups when the velocity of the center of mass is greater than the neutron CM velocity.

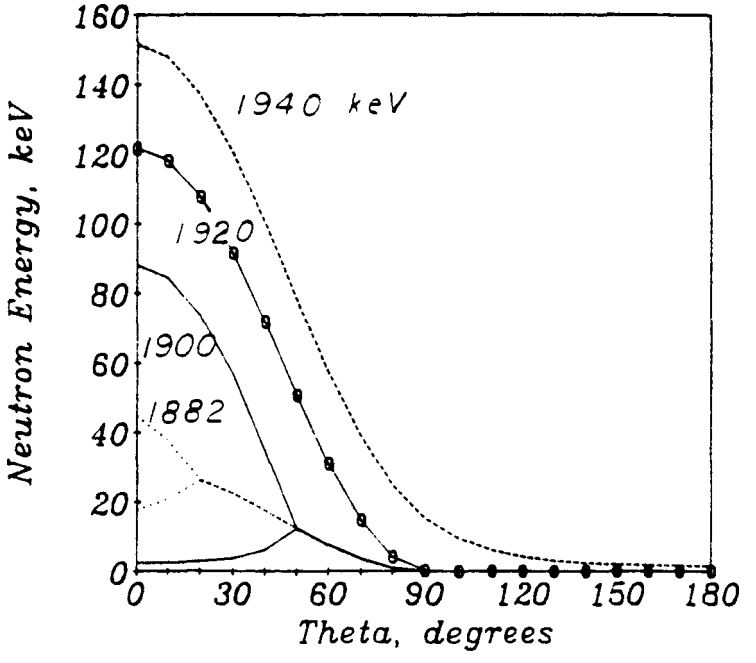

Fig. 11. Variation of neutron energy with laboratory angle, for various incident proton energies.

When the compound nucleus is moving faster than the neutron's center-of-mass (CM) velocity, then neutrons emitted at 180 degrees in the CM system will be moving forward at low energies in the lab system. Thus, there are two groups of neutrons at 0 degrees in the lab system: those emitted at 0 degrees in the CM system plus those emitted at 180 degrees in the CM system. This bifurcation is shown in Figure 11. At E_p = 1882 keV (near threshold) the bifurcation extends out to θ = 20 degrees. At 1900 keV it extends to 50 degrees, and at 1920 keV it disappears, because the neutron CM velocity is no longer less than the velocity of the center of mass. This same equation is shown in Figure 12. The bifurcation results in a peak of low-energy neutrons (~10 keV) in the forward direction.

Thick Target Neutron Yield

The neutron production can be calculated using a method similar to that used by Ottewitte [27] and by Clayton and Spackman [28]. Let I represent the proton beam intensity (protons/cm^{2}s). As the beam penetrates into the target, a few of the protons are destroyed by nuclear reactions, with the resulting beam attenuation represented by

$$I(x) = I_0 \exp\left[- \int_0^x dx\, n_{Li}\, \sigma \right],$$

where n_{Li} = 4.599E22 cm^{-3} is the lithium atom density, and σ is the total (p,x) cross section, dominated by the (p,n) reaction. To find the differential neutron source dY in terms of energy and angle, a differential cross section is used, where E_p, E_n and θ are related by Eq.(2):

$$dY(x,E_n,\theta) = I(x) n_{Li}\, \sigma_{pn}(E_p,\theta)\, d\omega\, dx\ .$$

In this equation dY has units of (neutrons/cm^{2}s), σ_{pn} has units of cm^2/steradian, and

$$d\omega = 2\pi \sin\theta d\theta$$

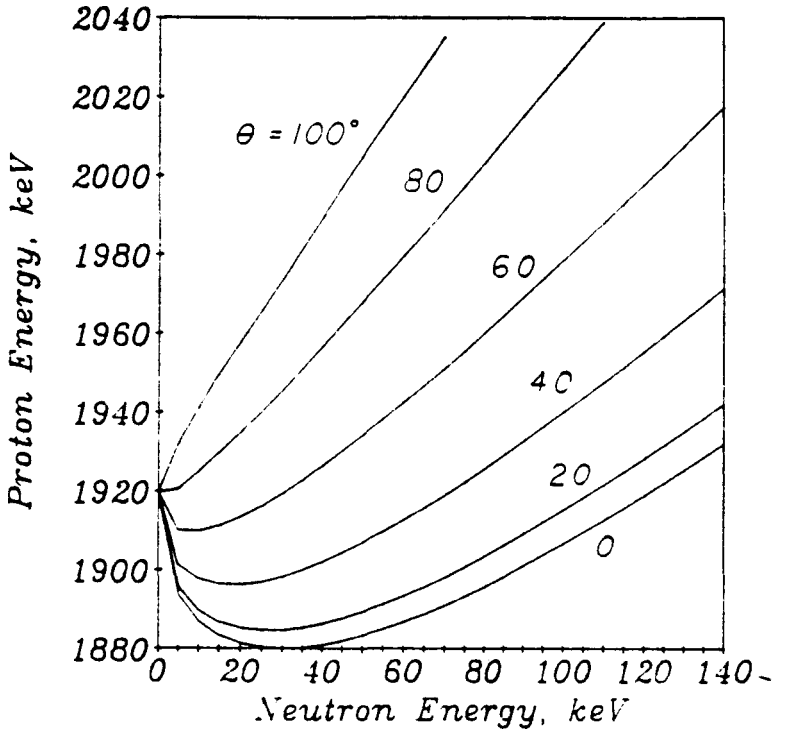

Fig. 12. Variation of proton energy with neutron energy, at various neutron lab angles.

is a differential solid angle. Dividing both sides by I_o gives the neutron yield per proton incident. This can be integrated over x to find the thick-target yield, as a function of energy and angle:

$$dY(E_n,\theta)/I_o = n_{Li} \int_0^R dx\ \sigma_{pn}(E_p,\theta)\ d\omega\ \exp[-\int_0^x dx\ n_{Li}\ \sigma\ ]$$

This is the basic equation to be solved.

Method of Integration

This equation may be simplified by noting that the argument of the exponential function is < 0.0002 (as found from the thick-target yield results), so that the exponential function's value is > 0.9998. Since the cross sections themselves are known only to about 5 % accuracy, the error < 0.02 % incurred by setting the exponential function equal to 1.00 is negligible.

The remaining integral could be evaluated using a range-energy curve to evaluate E_p at each x position. Alternatively, we can make the change of variables

$$dx = dE_p/(dE_p/dx)$$

to express the integral in terms of E_p:

$$dY(E_n,\theta)/I_o = n_{Li} \int_{E_{po}}^0 dE_p\ \ (dE_p/dx)^{-1}\ \ \sigma_{pn}(E_p,\theta)\ d\omega \qquad (4)$$

A set of angles θ and neutron energy groups ΔE_n are specified at the start of the calculation. Using Eq.(3), the bounding energies of a given neutron energy group (E_{n1},E_{n2}) are mapped to the corresponding proton energies (E_{p1},E_{p2}), which become the limits of integration for

finding the number of neutrons in that energy group. Care is taken to integrate along the direction of proton motion in the region of bifurcation. The numerical integration of each energy group is done by 10-point Gaussian quadrature, interpolating the differential cross section data with cubic splines.

Range-Energy Relationship

The range-energy relationship calculated from Eq.(1) is shown in Figure 13. These calculations have been tested in several ways:

(1) From Table 5 of Clayton and Spackman [28], the distance required to slow a proton from 2.5 MeV to 1.95 MeV is 4.432 mg/cm^2/(0.534 g/cm^3) = 83.0 μm, which compares with 81.7 μm in the present work.

(2) A range-energy curve was computed using the PRAL code, based on transport theory, which includes longitudinal and lateral straggling. It is part of the TRIM88 code [29,30]. The PRAL code has preset energy values, which do not include 2.5 MeV. It predicts a range of 216.2 μm at an energy of 2.4 MeV, which is comparable to the value of 221.8 μm predicted here.

(3) The TRIM code [29,30], based on the Monte Carlo technique, has been run to simulate 2.5 MeV protons in lithium. Using 1000 case histories, the results are:

mean range	=	236.0 μm
longitudinal straggling	=	3.43 μm
mean lateral spread of ions	=	6.11 μm

The present work predicts a range of 237.8 μm. The straggling and lateral spread is greatest near the end of the ion paths, where the energy is low. The protons will have slowed down to threshold energy after penetrating about 89 μm into the target, and only straggling in this depth will affect the (p,n) reaction rate calculations. The mean lateral spread at the end of the paths is about 2.6 % of the range, so it will probably be < 2 % at a depth of 89 μm. Similarly, the longitudinal

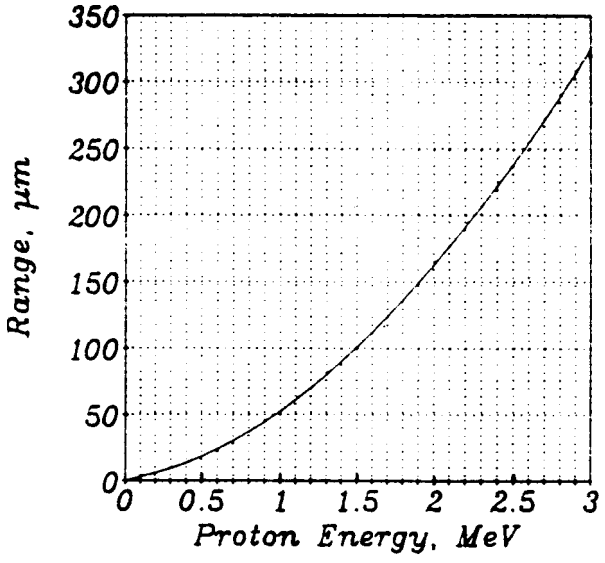

Fig. 13. Range vs. energy for protons in lithium.

straggling is 1.5 % at the end of the path, and probably < 1 % at 89 μm.

The neutron energy spectra calculated from Eq.(4) are shown in Figure 14 for a few representative emission angles. Integrating these curves over energy, we find the neutron source strength per proton-steradian as a function of angle, as shown in Figure 15. When this curve is integrated over all solid angles, the total neutron source strength from 2.5 MeV protons is found to be

$$Y/I_0 = 1.49\times10^{-4} \text{ neutrons/proton} = 9.3\times10^{11} \text{ neutrons/s-mA},$$

which is comparable to the value of 8×10^{11} quoted by Lone et al [31] and the value of 9×10^{11} obtained from Table 10 of Clayton and Spackman. [28]

Discussion

Some sources of error are listed in Table 7, using the estimates discussed above. These errors are expected to be random, rather than systematic. The cross section errors are greatest at E_p < 2 MeV. Accuracy at low energies could be improved by evaluating the cross sections using center-of-mass Legendre coefficients. Improved accuracy could also be obtained by using the TRIM code or the RAFFLE code with modifications to include nuclear reactions.

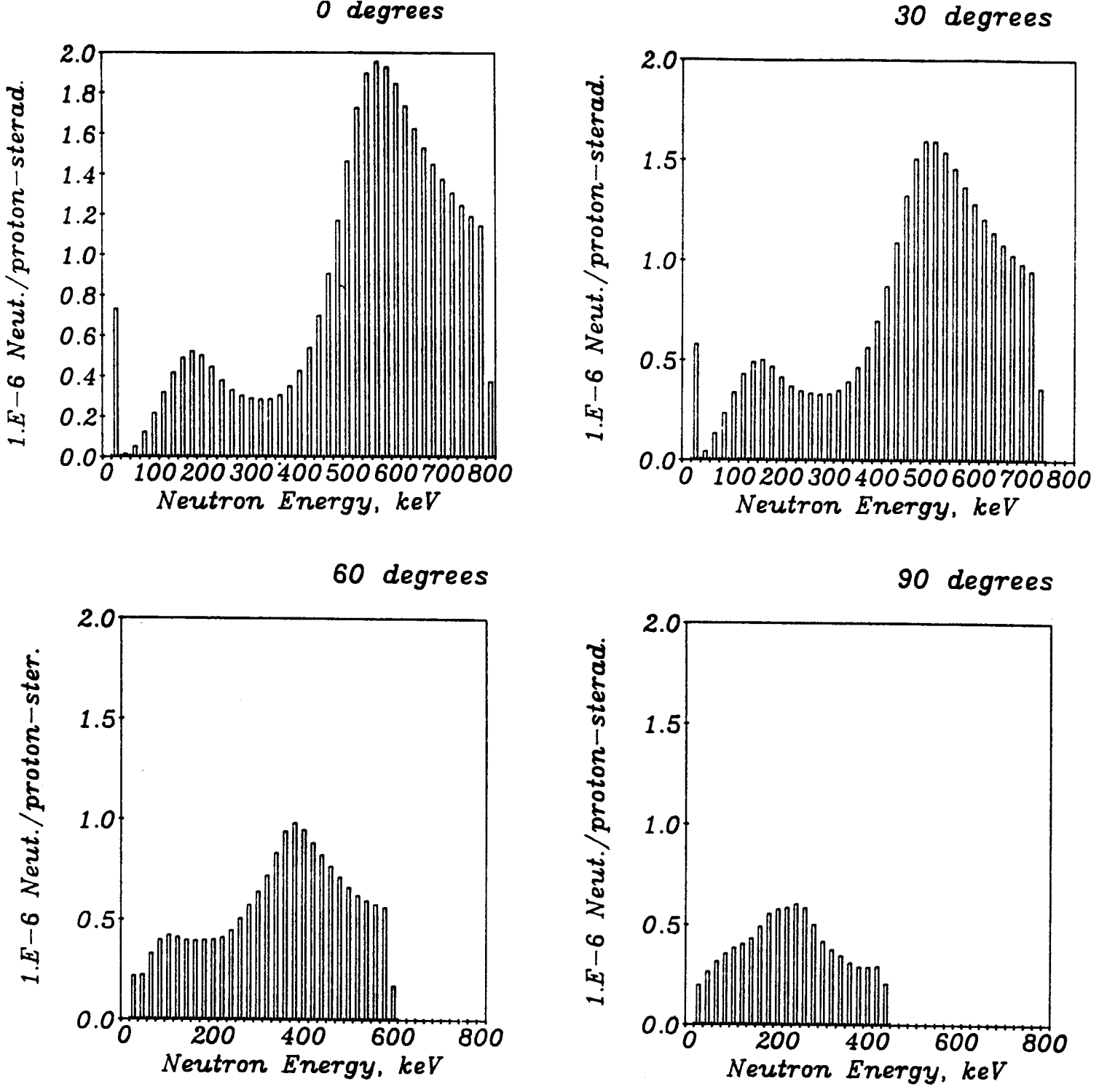

Fig. 14. Histograms of the differential neutron yield from the $^{7}Li(p,n)^{7}Be$ reaction at neutron emission angles of 0, 30, 60 and 90 degrees relative to the direction of the incident protons. Each bar shows the number of neutrons emitted in that 20 keV interval.

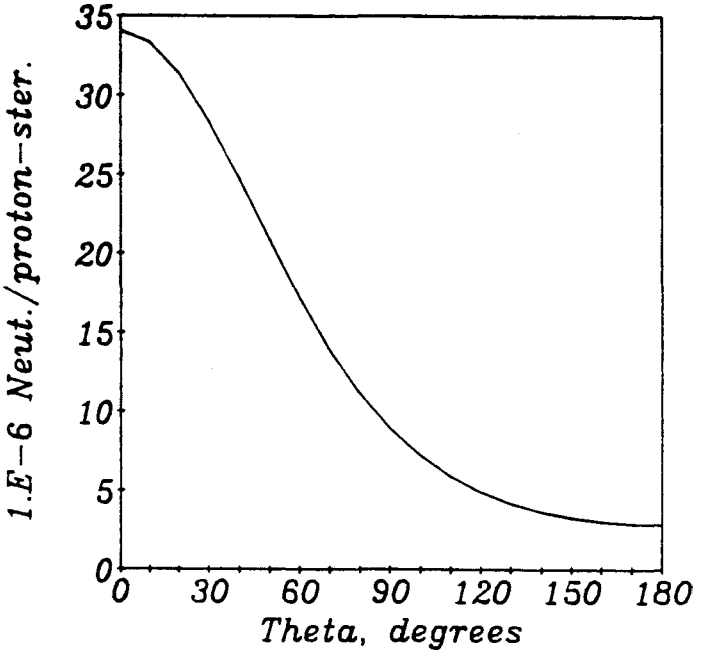

Fig. 15. Neutron source strength (neutrons/proton-steradian) as a function of neutron lab angle.

Table 7. Error Sources, Neutron Energy Spectrum Calculation.

Angular spread of proton beam	~ 3 degrees
Proton deflection in target	~ 1 degree
Deviation of incident protons from 2.5 MeV	< 1 %
Empirical equation for stopping power (including effects of straggling)	~ 2 %
Attenuation of proton beam in target by nuclear reactions	< 0.02 %
Neutron attenuation in target layer	< 0.06 %
Uncertainty of (p,n) cross section (greatest below 2 MeV	5-10 %
Cubic splines interpolation of cross section data	small
10-point Gaussian quadrature	small

Net error: angle ~ 3 degrees
energy ~ 5-10 %

4.2 Target Issues

The beam current should be maximized, in order to maximize the neutron flux at the patient and to minimize the required exposure time. The maximum beam current is limited by target heating, stress, and stability problems.

For a 40 mA, 2.5 MeV beam, the power incident on the target is 100 kW. The beam diameter at the target should be smaller than the patient's head, in order to avoid wasting neutrons produced at large radii. If we limit the beam radius to 10 cm, then the interaction area is 314 cm^2, and the average heat flux on the target is 318 W/cm^2.

The target surface could consist of either liquid lithium or LiF. Thin (5-10 mg/cm^2) lithium fluoride targets [16] have been used to produce monoenergetic neutrons at low beam currents (< 1 mA), but target lifetime for thick targets at high currents is dubious. A LiF target would have the following disadvantages, relative to a liquid lithium film:

a neutron yield much lower than pure Li
thermal conductivity (LiF) << thermal conductivity (Li)
    hence, much lower tolerable heat fluxes
thermal stress, adhesion and flaking problems.

For these reasons, LiF is not considered further here.

One obvious target design is a thin Li film on a metal substrate, illustrated in Figure 16. In order to keep the Li vapor pressure < 0.013 Pa (10^{-4} Torr), the surface temperature of the Li should be kept below 400 C. For a heat flux of 318 W/cm^2, this surface condition is satisfied by a Be substrate 5 mm thick with a 1 mm Li film, cooled by water at 1 MPa (10 atm) flowing at 5.6 m/s.[31] For a beam diameter of 20 cm, the corresponding 2.5 MeV beam current would be limited to 40 mA. Hence, a current of 40 mA is assumed in estimating the neutron source strength and patient exposure in this report. However, higher currents may be attained by use of innovative target designs.

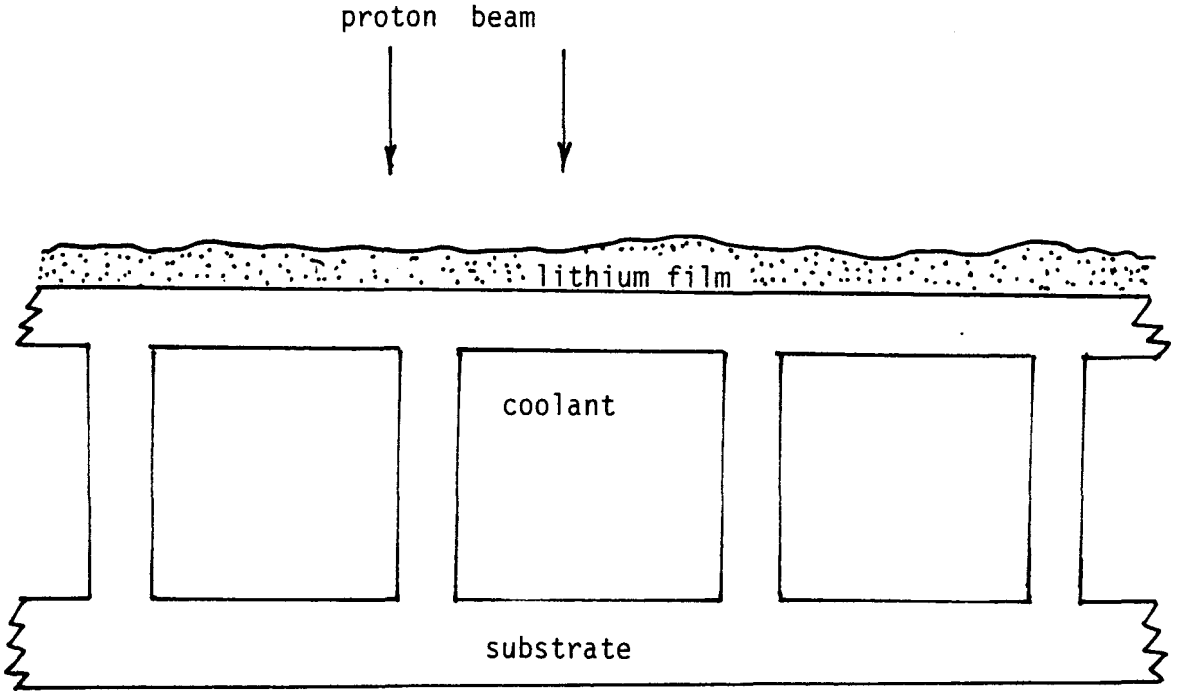

Fig. 16. A metal substrate target design. [31]

Lithium has a high surface tension, which would make it tend to form droplets, instead of wetting the surface. One possible way to solve this problem is illustrated in Figure 17. Here the Li film is maintained on the inside of a rotating drum by centrifugal force. The high surface tension of Li would thus be compensated by an increased effective value of g, the gravitational constant. With a drum radius of 30 cm, a rotational speed of 3 Hz (200 rpm) would produce an acceleration of about 10 g, which should make the wetting similar to that of water. The rotation would also increase the allowable heat flux and beam current.

It might be feasible to use a pool of molten lithium as the target. The pool could maintain its integrity more easily than a thin coating on a substrate, but heat removal would be largely by vaporization of the lithium, with recondensation on the sides of the vessel.[32] In order to prevent contamination of the accelerator by streaming lithium, an elaborate cold trap, including bends of the beam line, would be needed. According to Gibbons and Newson [16], "Lithium metal is, of course, the ideal form, but it is so chemically active that elaborate steps, to be discussed later in this section, must be taken in order to both produce and maintain a clean target."

Another attractive possibility is a flowing lithium "waterfall" type of target, as proposed for the Fusion Materials Irradiation Test (FMIT) Facility. This target was designed to withstand bombardment by 100 mA of 35 MeV deuterons, without excessive backflow of lithium vapor to the accelerator.[33] This power deposition is equivalent to 1400 mA of protons at 2.5 MeV. The flowing lithium could have a lower temperature and vapor pressure than the lithium in a pool target. An adaptation of the FMIT target design for BNCT use is needed.

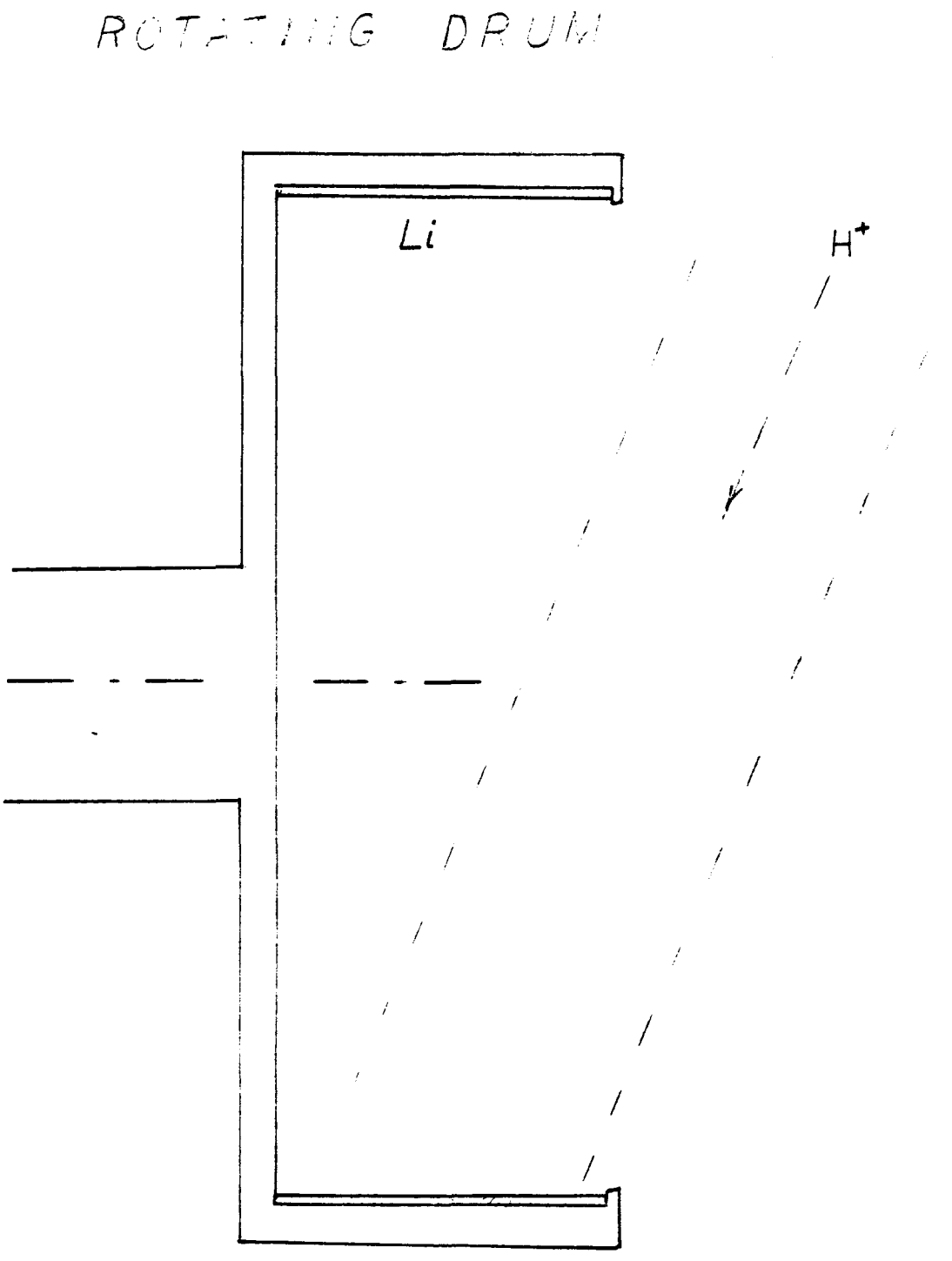

Fig. 17. A rotating drum to keep the lithium film spread over the surface of the substrate.

4.3 Gamma Ray Production

There are several ways in which gamma rays are produced by the $^{7}Li(p,n)^{7}Be$ reaction:

* capture of neutrons in the target, filter, shielding, patient, etc.
* electromagnetic decay of excited states $^{7}Be^{*}$
* $^{7}Li(p, p' \gamma)$ inelastic reactions (0.48 MeV)
* $^{6}Li(p, p' \gamma)$ inelastic reactions
* $^{7}Li(p, \gamma)$ capture reactions (15-20 MeV)
* $^{6}Li(p, \gamma)$ capture reactions
* delayed gammas from decay of the ^{7}Be back into ^{7}Li

The neutron-induced capture gammas are determined later in the neutron transport calculations. Here we assume that $E_p < 2.6$ MeV, so that $^{7}Be^{*}$ excited state production is negligible.

Gamma Flux

For a point source S (gammas/s) passing through a slab with thickness R and attenuation coefficient μ, the resulting gamma flux is given approximately by

$$\phi_\gamma = B\ S\ \exp(-\mu R)/4\pi R^2,$$

where B is the buildup factor. The gamma flux equivalent to 1 rem/hr (1 cGy/hr) is $10^6/cm^2s$ at 0.5 MeV and $8x10^4/cm^2s$ at 15 MeV.[34]

Li(p, p' γ) Reactions

According to Antilla et al [35], the 0.478 MeV gamma yield from inelastic proton scattering in ^{7}Li is $260x10^5$ gammas/μC-sterad at $E_p = 2.4$ MeV. Assuming isotropic distribution, this would be $3.3x10^8$ gammas/μC, or $3.3x10^{11}$ gammas/s-mA at 2.4 MeV. A current I = 0.04 A would yield S = $1.3x10^{13}$ gammas/s. This yield can also be estimated from data of Barker [36], indicating a cross section ~ 70 mb. Assuming a distance d ~ 180 μm for gamma production, the gamma yield

$S \sim (I/e)n_{Li}\sigma\, d = 1.4\times10^{13}$ gammas/s,

at 40 mA, which is consistent with the previous estimate. Here e is the charge of the proton, and n_{Li} is the lithium atom density. For 0.5 MeV gammas in 20 cm of BeO, $\mu = 0.251/cm$, $\mu R = 5.01$, $B \sim 20$, and the gamma flux $\phi_\gamma(R) = 2.7\times10^{-5}S = 3.8\times10^{8}$ gammas/cm^{2}s. This flux would produce a dose rate of 380 rem/hr (3.8 Gy/hr), and additional gamma shielding would be desirable. Cross sections for inelastic scatter in ^{6}Li have not yet been found.

Li(p,γ) Reactions

Lithium-6 has a (p,γ) cross section of only 6 μb at 2 MeV.[37] This would produce a negligible dose to the patient.

The lithium-7 yield of 15-20 MeV photons quoted by Fowler et al [38] is $eS/I = 1.9\times10^{-8}$ gammas/proton, which would yield $S = 4.7\times10^{9}$ gammas/s at I = 40 mA. However, a resonance cross section $\sigma \sim 6$ mb is given by Golicheff et al.[39] Assuming d = 180 μm, this cross section would give $S \sim 1.2\times10^{12}$ gammas/s, which is about 260 times higher.

At 15-20 MeV in BeO, $\mu = 0.049/cm$, $\mu R = 0.98$, $B \sim 1.3$, and $\phi_\gamma = 10^{-4}S$. The source based on Golicheff's cross section would yield $\phi_\gamma = 1.2\times10^{8}$ gammas/cm^{2}s, corresponding to a dose rate ~ 1500 rem/hr; but the source based on Fowler's data would yield a dose rate ~ 5.9 rem/hr. This discrepancy may be due in part to inaccurate equipment used in the 1940's, and in part to the 6 mb cross section being a resonance peak, not an average cross section. The (p,γ) source term needs further study.

Decay Gammas from ^{7}Be

Beryllium-7 decays by electron capture with a half life of 52.28 days into ^{7}Li. A fraction $\alpha = 0.103$ of these events results in gamma ray emission with energy 0.4776 MeV. The ^{7}Be can also be destroyed by

neutron absorption, with a cross section of 54,000 b (thermal). If we let N = total number of ^{7}Be atoms in the target, its variation can be represented by the equation

$$dN/dt = yI/e - \lambda N - N \int dE\ \sigma(E)\ \phi_n(E) \equiv yI/e - \beta N$$

where I is the proton current (A), e is the proton charge, y is the yield (^{7}Be atoms per proton), λ is the ^{7}Be decay constant, $\sigma(E)$ is the neutron capture cross section of ^{7}Be at neutron energy E, $\phi_n(E)$ is the energy-dependent neutron flux, and β combines the last two terms. Assuming no ^{7}Be is initially present in the target, the resultant activity A after irradiation for a time t is

$$A(t) = \alpha\lambda N = (\alpha\lambda yI/e\beta)[1 - \exp(-\beta t)]$$

Consider operation with a sequence of irradiation periods t_i followed by setup times t_s, as illustrated in Figure 18. The resultant activity builds up as shown in the bottom graph. At the end of 1 irradiation, the activity is

$$A_1 = (\alpha\lambda yI/e\beta)[1 - \exp(-\beta t_i)].$$

After the second irradiation, this activity has decayed by $\exp[-\lambda(t_s + t_i)]$, and some new ^{7}Be atoms have been added, with the result that

$$A_2 = A_1 \exp[-\lambda(t_s + t_i)] + A_1.$$

By induction, the activity after n irradiation cycles is found to be

$$A_n = A_1 \sum_{k=0}^{(n-1)} \exp[-k\lambda(t_s + t_i)] \simeq nA_1\ [1 - 0.5(n-1)\lambda(t_s + t_i)].$$

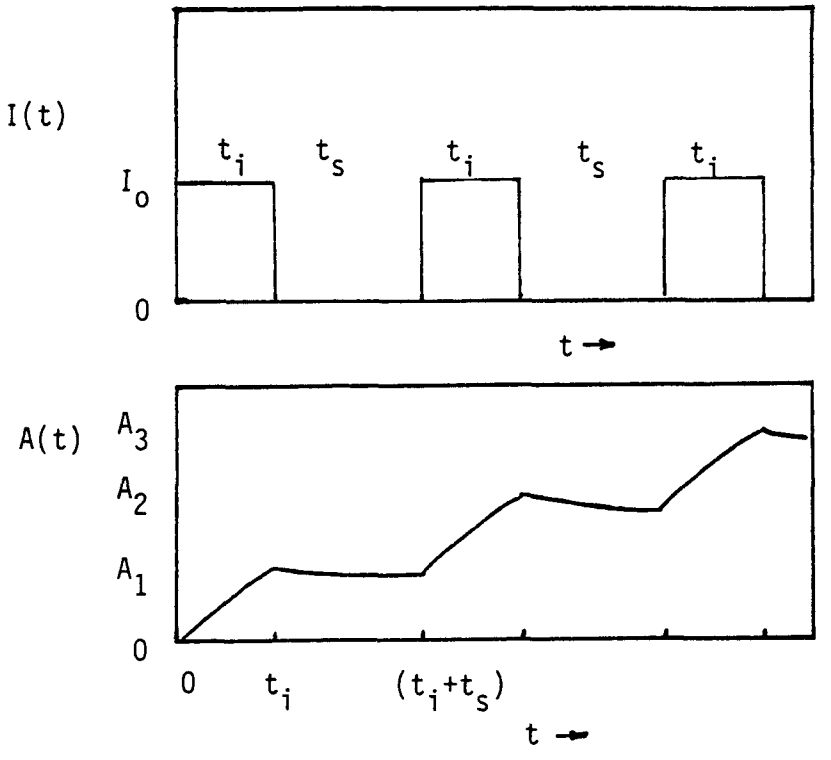

Fig. 18. Proton beam current vs. time (top) and resultant target activity vs. time (bottom), arbitrary units.

The latter equality is valid when the arguments of the exponential functions are small (when the total irradiation time is less than a week). The activity can be kept below dangerous levels by frequently replacing the lithium target with unirradiated lithium, and the radioactive targets can be recycled after decaying for many half lives.

To illustrate the gamma activity, consider a case in which I = 40 mA, $t_i = t_s$ = 30 minutes, and n = 8 cycles. Since the target is very thin, the source neutrons (0-780 keV) easily escape, and the thermal neutron flux may be significantly lower than the source flux. Then the destruction of ^{7}Be by neutrons may only be a few percent of its radioactive decay rate λ. For simplicity, we will assume that

$$\beta \sim \lambda.$$

If destruction of ^{7}Be is significant, then the target activity will be lower than estimated using this conservative approximation.

The resulting target activity after 8 cycles is found to be

$$A_8 \simeq 8\alpha\lambda t_i I/e = 8.4\times10^9 \text{ Bq}$$

This source strength would produce a flux $\phi_\gamma = 2.2\times10^5/\text{cm}^2\text{s}$ outside the 20 cm BeO slab, corresponding to a dose rate of 0.22 rem/hr.

Summary

The target gamma activity due to decay of ^{7}Be can be kept small by replacing the target lithium about once a week. The prompt gamma activity from (p, p' γ) reactions at I = 40 mA is estimated to be ~ 380 rem/hr, which would require additional shielding. The prompt gamma activity from (p,γ) reactions is in doubt, due to inconsistent data in the literature, but it could be as large as 1500 rem/hr.

4.4 Neutron and Gamma Fluxes at the Patient with a BeO Filter

The neutronics calculations use the DOT4.3 discrete ordinates code with S8 quadrature.[40] The BUGLE-80 coupled neutron-gamma P_3 cross section set, consisting of 47 neutron energy groups and 20 gamma energy groups, is used.[41] The neutron filter and shield studied is shown in Figure 19. The 20 cm BeO filter is covered with a thin layer of lithium, to reduce the thermal neutron dose, and surrounded by an alumina reflector. This represents the design of the Ohio State University group, for comparison with their results.[4] The calculation utilizes the energy and angle-dependent neutron source derived in Section 4.1. The target was assumed to be an infinitely thin disk 5 cm in diameter. The substrate and coolant were not treated. The gamma dose from the target was estimated in Section 4.3, and only gammas resulting from absorptions in the neutron filter and shield are included here.

Several results of the neutron transport calculations are of interest for patient treatment. These are the energy spectrum, intensity, angular divergence and spatial variation of the neutron flux at the patient treatment location, shown in Figure 19. The energy spectrum and flux intensity are of primary importance in determining the suitability of the accelerator system for BNCT.

Figure 20 shows the resulting neutron energy spectrum for the accelerator system (at a lower current), together with the spectra from two Medical Therapy Reactor (MTR) conceptual designs.[3] The accelerator spectrum was taken at the leakage surface past the BeO filter shown in Figure 19.

The present accelerator yields an epithermal neutron flux, but the flux contains a significant fast and thermal contaminant. Approximately 30 % of the total flux is outside the epithermal range, compared with < 10 % for the MTR concepts. The flux intensities of the accelerator and MTR also differ. The design criterion for the MTR is a neutron flux

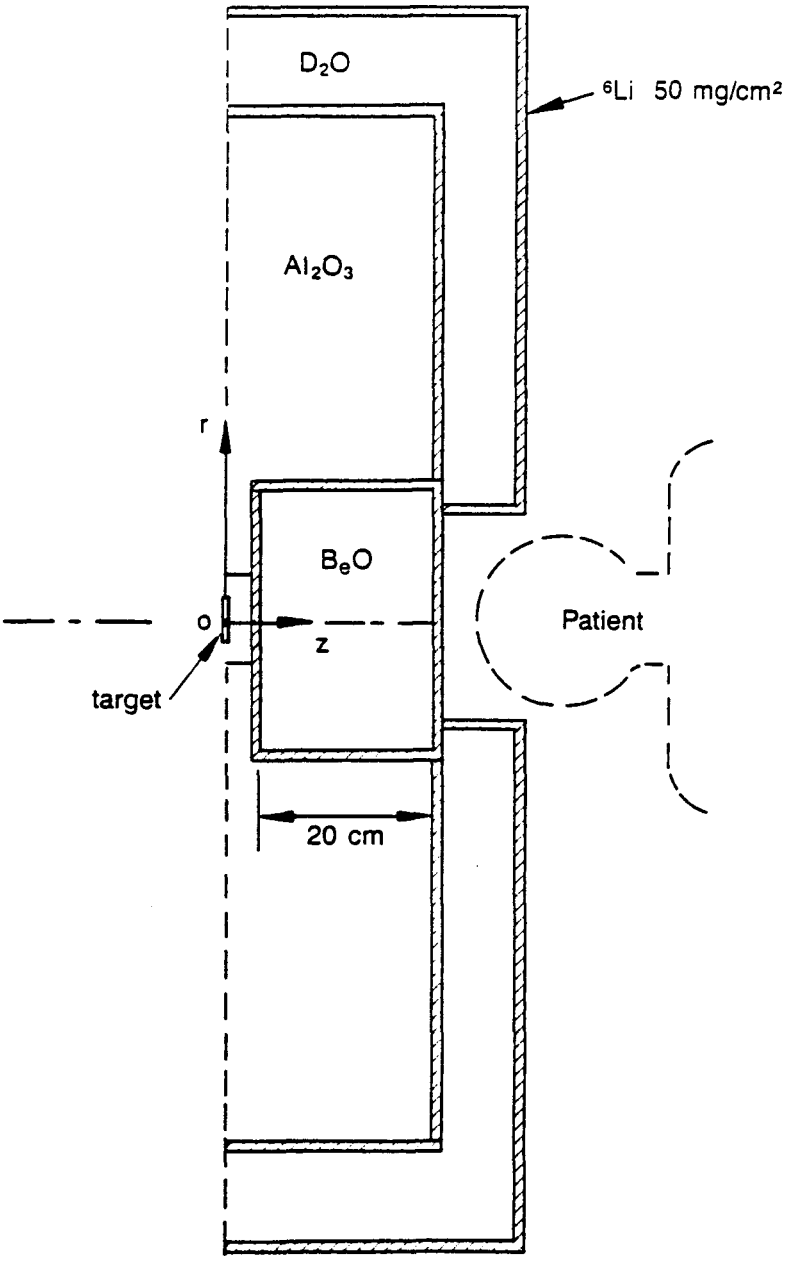

Fig. 19. Arrangement of filter and shield, patient and target locations. Based on design of Ref.[42].

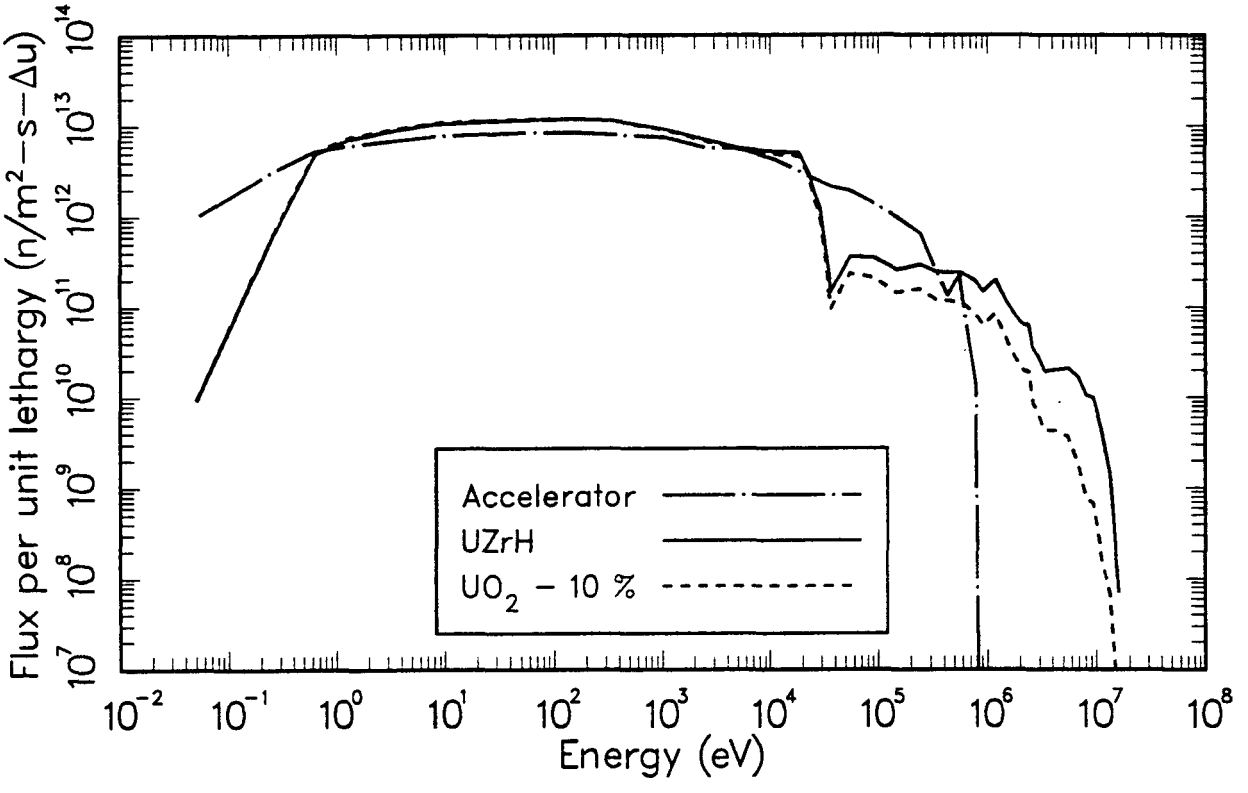

Fig. 20. Neutron energy spectra for the $^{7}Li(p,n)$ reaction (proton current ~ 100 mA, filter = 20 cm BeO) and for the medical therapy fission reactor.[3]

of 10^{14} neutrons/m^2s.[3] The accelerator source at 10 mA produces a flux of ~ $10^{13}/m^2$s. This is higher than the Ohio State group calculation of 4.9 x $10^{12}/m^2$s at 10 mA.[4] The difference may be due to the location where the flux is measured, since the flux intensity decreases rapidly with distance away from the filter. Thus, it would be desirable to place the patient as close to the filter as possible.

Having calculated the flux intensity, the fast neutron and gamma contaminants of the beam during patient treatment can be found. A treatment consists of a total neutron fluence of $6x10^{16}$ neutrons/m^2. This would take 10 minutes with the MTR, or 50 minutes with the accelerator at 20 mA. The fast neutron KERMA for the treatment period is ~ 2 Gy, compared to 1.2 Gy for an unoptimized oxide-fueled MTR (and lower for an optimized MTR). The gamma contaminants from neutron capture, $(p,p'\gamma)$ reactions, and (p,γ) reactions are 1.1 Gy, 1.6 Gy, and 2-6 Gy (cross section uncertain), respectively, compared to 0.2 Gy for the MTR concept. The total of 5.7-9.7 Gy divided by the number of source neutrons (1.86 x 10^{13} n/s for 50 min) is 1.0-1.7 x 10^{-16} Gy per source neutron, which is consistent with the value of 1.1 x 10^{-16} Gy per source neutron shown in Fig. 15 of Ref.[4]. These contaminant levels would probably require additional filtering or shielding, which would reduce the achievable neutron intensity of the accelerator system.

The spatial variation of the flux at the patient treatment location is important because of the uncertainty in the location of the multiple tendrils produced by Glioblastoma Multiforme tumors. A flat radial profile across the BeO leakage face is desired to ensure all parts of the tumor will be subjected to sufficient neutron bombardment. The average beam intensity determines the usable epithermal flux, while the peak beam intensity determines the maximum dose to healthy tissue. The accelerator source results in a ratio ϕ_{max}/ϕ_{min} = 1.46 across the BeO leakage face, compared to a ratio = 1.10 for the MTR. The effect of this spatial variation on the treatment of distributed tumor regions needs to be addressed. The accelerator ratio could be improved by using a larger target diameter, at the expense of a decreased flux intensity.

The last quantity of interest is the degree to which the patient treatment flux can be collimated after being filtered into the epithermal energy range. The level of benefit derived from a perfectly collimated beam, compared with a disperse or isotropic flux, is not well quantified and depends on the location of the tumor mass. A well collimated beam is generally considered to be beneficial for treatment, and it is certainly advantageous for neutron economy. The accelerator filter configuration does not attempt to collimate the neutron flux, and the flux/leakage current is ~ 2 (isotropic distribution) at the BeO leakage face. The MTR neutron flux is collimated after moderation into the epithermal range and has a resulting flux/leakage current ~ 1.35 at the patient location. For a perfectly collimated beam, the flux/leakage current ratio would be unity.

The maximum cw beam current attained by RFQ accelerators is about 20 mA. The accelerator neutron source parameters at this current are compared with the Medical Therapy Reactor neutron beam in Table 8.

The 20 mA accelerator produces a flux intensity 5 times lower than the proposed MTR fission reactor, and has a much greater fast neutron and gamma contaminant than the MTR spectrum, so additional shielding would be required. This additional shielding would further reduce the neutron intensity. The utility of the accelerator source will also depend on the tolerance of patient treatment to the large spatial and angular variations in the leakage flux. The MTR facility has better radial flatness and collimation of the treatment beam.

Table 8. Comparison of a 20 mA accelerator neutron source with a Medical Therapy Reactor for BNCT applications.

	accelerator	reactor
Flux at patient, $10^{13}/m^2s$	< 2	10
Treatment time, minutes	> 50	10
Flux/current ratio	2 (divergent)	1.35 (collimated)
Max/min flux from filter	1.46 (nonuniform)	1.10 (uniform)
Fast neutron KERMA, Gy	2-3	1.2-1.7
Gamma dose, Gy	3-9 (too high)	0.2

5.0 Summary and Conclusions

Of all the reactions surveyed, the $^{7}Li(p,n)$ reaction appears to be the most favorable for producing high fluxes of epithermal neutrons. Reactions with heavier elements, such as Sc, can produce epithermal spectra with low maximum neutron energies (~ 10 keV), but have yields an order of magnitude lower.

For a target diameter of 20 cm, heat transport considerations limit the current of 2.5 MeV protons to about 40 mA with a static lithium film on a water-cooled metal substrate. Higher currents would probably be tolerable on a rotating target or on an FMIT type of flowing lithium target. For producing high currents of 2.5 MeV protons, the RFQ accelerator is the most compact and economical. A medical accelerator might be designed to fulfill a dual role: BNCT and radioisotope production.

The neutron flux obtained for the $^{7}Li(p,n)$ reaction with a 20 cm BeO filter is consistent with the results obtained by the Ohio State group. In comparison with a medical therapy fission reactor, a 20 mA accelerator system has

* a flux intensity at least 5 times lower, requiring an irradiation time at least 5 times longer,
* a much higher gamma intensity, which would probably require additional shielding, further reducing the neutron intensity,
* 30 % of the neutrons above 15 keV (vs. <10 % for the reactor), resulting in a higher fast neutron dose to healthy tissue,
* poorer spatial uniformity of the neutron beam, and
* greater angular divergence of the neutron beam (poorer collimation), resulting in a rapid decrease of flux with distance from the filter.

The possibility of overcoming these limitations by using more shielding and a higher beam current needs further study. RFQ accelerator technology is being developed to provide the desired proton beam parameters (~ 100 mA at 2.5 MeV). The effects of neutron beam energy spectra, beam contaminants, angular divergence, spatial variation, and beam rotation around the tumor need to be studied in detail, in order to optimize the effectiveness of BNCT for tumors at various depths.

The following tasks are proposed for future work:

1. Do a comprehensive study of neutron transport in tissue phantoms to determine the optimum neutron energies for BNCT, as functions of tumor depth and type.
2. Do detailed target design studies, including heat removal, induced radioactivity, vapor pressure, and target replacement procedures for candidate target designs. Adapt the FMIT target to BNCT applications. Determine the beam current and neutron production rate.
3. Improve the gamma dose rate estimates and the filter and shield design. Clarify the effects spatial and angular variations, high-energy neutrons, and gamma rays on the utility of accelerator-produced neutrons for patient treatment. Determine the time required for patient therapy.
4. Design an accelerator-based BNCT facility. Estimate the capital cost, operating cost, and cost per patient.

6.0 REFERENCES

1. H. Hatanaka, "Clinical experience of boron-neutron capture therapy for malignant brain tumors", Use and Development of Low and Medium Flux Research Reactors, Proceedings of the International Symposium, MIT, Oct. 16-19, 1983, O. K. Harling et al, Editors, Karl Thiemig, Munich, 1984, p.47-54.

2. D. K. Parsons, F. J. Wheeler, B. L. Rushton, and D. W. Nigg, "Neutronics design of the INEL facility for boron neutron capture therapy clinical trials", Proceedings of the 1988 International Reactor Physics Conference, Jackson Hole, WY, Sep.18-22 1988, Vol. 2, p. II-433 (ANS, 1988).

3. W. A. Neuman, D. K. Parsons, J. A. Lake, "Neutronics design of a Medical Therapy Reactor", Proceedings of the 1988 International Reactor Physics Conference, Jackson Hole, WY, Sep.18-22, 1988, ANS, 1988, Vol.2, p. II-443.

4. C.-K. C. Wang, T. E. Blue, R. Gahbauer, "A neutronic study of an accelerator-based neutron irradiation facility for boron neutron capture therapy", Nuclear Technology 84, 93-107 (1989).

5. F. J. Wheeler, INEL Letter Whlr-22-87 to R. Fairchild, Dec. 22, 1987.

6. R. G. Fairchild, "Recent advances in neutron capture therapy (NCT)", Exploration of the Possibility of High LET Radiation for Non-Conventional Radiotheraphy in Cancer, IAEA-TECDOC-396, Vienna, 1986.

7. Y. Oka et al., "Design of Facilities for BNCT-Epithermal Neutron Sources", BNCT for Tumors, H. Hatanaka (Ed.), Nishimura, 1986, Japan, p.247.

8. K. Morstin, B. Kawecka, and L. E. Feinendegen, "Remarks on the optimization of incident neutron energy for neutron capture therapy", Proceedings of the First International Symposium on Neutron Capture Therapy, R. G. Fairchild and G. L. Brownell, Eds., BNL-51730 (1982).

9. C-K. C. Wang, T. E. Blue, and R. A. Gahbauer, "A design study of an accelerator-based epithermal neutron source for boron neutron capture therapy", Proceedings of the Third International Symposium on Neutron Capture Therapy, Bremen, FRG, 1988.

10. H. Conde, et al., "Time of Flight Measurements of the Energy Spectrum of Neutrons Emitted from a Spallation Source and Moderated in Water," Nucl. Instruments and Methods in Physics Research A261 (1987), 587-90

H. Conde, et al., "The Production by 72 MeV Protons of keV Neutrons for ^{10}B Neutron Capture Therapy," Proc. of the Sixth Symposium on Neutron Dosimetry, Neuherberg, F.R.G. 12-16 October 1987, to be published; also SIN Medical Newsletter No. 9, 1987 (EDF-MED-19).

H. Conde, et al., "The Production of keV Neutrons by 72 MeV Protons," Proc. of the Third International Symposium on Neutron Capture Therapy, Bremen, F.R.G., 31 May-3 June 1988, to be published.

11. Y. Maruyama, J. Lawrence Beach and Jose M. Feola (Eds.), Californium-252 Brachytherapy and Fast Neutron Beam Therapy, Proceedings of the Workshop Held in Lexington, Kentucky, April 21-24, 1985, Nuclear Science Applications Section B 2 (3), 1986.

12. R. J. Howerton, "Thresholds and Q values of nuclear reactions induced by neutrons, protons, deuterons, tritons, He-3 ions, alpha particles, and photons", UCRL-50400-Volume 24, March 25, 1981.

13. F. W. Walker et al, "Chart of the Nuclides", 13th Edition, General Electric Company, 1984.

14. H. T. Richards, R. V. Smith, C. P. Browne, "Proton-neutron reactions and thresholds", Phys. Rev. 80, No. 4, 524-530 (1950).

15. J. E. Brolley, Jr. and J. L. Fowler, "Monoenergetic neutron sources: reactions with light nuclei", in Fast Neutron Physics, Part I, J. B. Marion and J. L Fowler, Eds., Interscience, NY, 1960 , p. 73-111.

16. J. H. Gibbons and H. W. Newson, "The $Li^7(p,n)Be^7$ reaction", in Fast Neutron Physics, Part I, J. B. Marion and J. L Fowler, Eds., Interscience, NY, 1960 , p. 133-176.

17. J. H. Gibbons and R. L. Macklin, "Total neutron yields from light elements under proton and alpha bombardment", Phys. Rev. 114, No. 2, 571-580 (April 15, 1959).

18. J. B. Marion, "Monoenergetic neutron sources", in Fast Neutron Physics, Part I, J. B. Marion and J. L Fowler, Eds., Interscience, NY, 1960, p. 113-132.

19. Marion, Bonner and Cook, Physical Review 100, 847 (1955).

20. H. Liskien and A. Paulsen, "Neutron production cross sections and energies for the reactions $^7Li(p,n)^7Be$ and $^7Li(p,n)^7Be^*$ ", Atomic Data and Nuclear Data Tables 15, No 1, 57-84 (January, 1975).

21. W. Scharf, Particle Accelerators and Their Uses, Harwood Academic, New York, 1986.

22. B. Smathers and L. T. Myers, "Use of cyclotrons in medical research: past, present, future", Nuclear Instruments and Methods in Physics Research B10/11, 1111-1116 (1985).

23. W. Beecraft et al, "RF accelerated high energy (1-3 MeV) neutral beams for tokamak plasma heating, current drive and diagnostics", Proceedings of the Eighth Topical Meeting on the Technology of Fusion Energy, Salt Lake City, Oct.9-13, 1988.

24. D. I. Garber and R. R. Kinsey, Neutron Cross Sections, Vol. 2 Curves, BNL-325, 3rd Edition, Jan. 1976.

25. H. H. Andersen and J. F. Ziegler, Hydrogen Stopping Powers and Ranges in All Elements, Vol. 3 of The Stopping and Ranges of Ions in Matter, Pergamon Press, New York, 1977.

26. R. D. Evans, The Atomic Nucleus, McGraw-Hill, New York, 1955, p.412.

27. E. H. Ottewitte, "Interaction of 200- and 175-keV deuterons with tritium-loaded titanium", INEL Internal Report RE-P-81-013, 1981.

28. C. G. Clayton and R. Spackman, "Neutron intensity and energy distributions from protons in the energy range 1.95 MeV to 5.5 MeV incident on thick targets of lithium", Int. J. Appl. Radiat. Isot. Vol. 36, No. 1, 13-50 (1985).

29. J. F. Ziegler, J. P. Biersack and G. Cuomo, "TRIM88" computer code to calculate slowing down of ions in solids by transport and Monte Carlo methods.

30. J. F. Ziegler, J. P. Biersack and U. Littmark, The Stopping and Range of Ions in Solids, Vol. 1 of The Stopping and Ranges of Ions in Matter, Edited by J. F. Ziegler, Pergamon Press, New York, 1985. This book provides a listing and explanation of TRIM85, and earlier version of TRIM88.

31. M. A. Lone, A. M. Ross, J. S. Fraser, S. O. Schriber, S. A. Kushneriuk, and W. N. Selander, "Low energy $^{7}Li(p,n)^{7}Be$ neutron source (Canutron), Chalk River Laboratories Report AECL-7413 (1982).

32. J. W. Blue, W. K. Roberts, T. E. Blue, R. A. Gahbauer, and J. S. Vincent, "A study of low energy proton accelerators for neutron capture therapy", Proceedings of the Second International Symposium on Neutron Capture Therapy, Teikyo University, Tokyo, Oct.18-20, 1985.

33. R. R. Miles, R. K. Greenwell, J. A. Hassberger, J. G. Ingham, "Improved liquid-lithium target for the FMIT facility", Transactions of the American Nuclear Society 43, 193 (1982).

34. J. R. Lamarsh, Introduction to Nuclear Engineering, Addison Wesley, Reading, MA, 1983.

35. A. Antilla, R. Hanninen, J. Raisanen, "Proton-induced thick-target gamma-ray yields for the elemental analysis of the Z =- 3-9, 11-21 targets", J. Radioanal. Chem. 62, 293-306 (1981).

36. F. C. Barker, "2^- States of ^{8}Be", Australian Journal of Physics 30, 113-125 (1977).

37. F. C. Barker, "Neutron and proton capture by ^{6}Li", Aust. J. Phys. 33. 158-176 (1980).

38. W. A. Fowler, and C. C. Lauritsen, "Gamma-radiation from light nuclei under proton bombardment", Physical Review 76, 314 (1949).

39. I. Golicheff, M. Loeuillet, and Ch. Engelmann, "Analytical application of the direct observation of nuclear reactions induced by low-energy protons and leading to the emission of gamma-photons, which are measured", Journal of Radioanalytical Chemistry 12, 233-250 (1972).

40. W. A. Rhoades and R. L. Childs, "An updated version of the DOT4 one- and two-dimensional neutron/photon transport code", ORNL-5851, Oak Ridge National Laboratory, 1982.

41. R. W. Roussin, "BUGLE-80, coupled 47-neutron, 20 gamma ray, P_3 cross-section library for LWR shielding calculations", DLC-75, Radiation Shielding Information Center, 1980.